Functional single-cell genomics of human cytomegalovirus infection

Marco Y. Hein[1,✉] and Jonathan S. Weissman[1,✉]

[1]Department of Cellular and Molecular Pharmacology & Howard Hughes Medical Institute, University of California San Francisco, San Francisco CA 94143, USA

Understanding how host factors and hundreds of viral genes orchestrate the complex life cycle of herpesviruses represents a fundamental problem in virology. Here, we use CRISPR/Cas9-based screening to scan at high-resolution for functional elements in the genome of human cytomegalovirus (HCMV), and to generate a genome-wide mapping of host dependency and restriction factors. Our data reveal an architecture of functional modules in the HCMV genome, and host factor pathways involved in virus adhesion and entry, membrane trafficking, and innate immune response. Single-cell analysis shows that the large majority of cells follow a stereotypical trajectory in viral gene expression space. Perturbation of host factors does not alter this trajectory, but can accelerate or stall progression. Conversely, perturbation of viral factors creates discrete alternate 'dead-end' trajectories. Our results reveal a fundamental dichotomy between the roles of host and viral factors in orchestrating viral replication and more generally provide a road map for high-resolution dissection of host-pathogen interactions.

Correspondence: ***marco.hein@ucsf.edu, jonathan.weissman@ucsf.edu***

The betaherpesvirus HCMV is a pervasive pathogen that establishes lifelong infection in the majority of the human population. Activation of its lytic cycle triggers a characteristic cascade of events, starting with stereotypical waves of viral gene expression, continuing with the replication of the large, 235 kb dsDNA genome, and culminating in the budding of newly assembled virions. A number of systematic studies have described these phenomena on the level of the transcriptome, the set of translated messages, and the proteome in time and space (1–6). These studies have highlighted the complexity of the process and have raised the question of how hundreds of viral genes cooperate to manipulate the host and undermine its defense machinery. CRISPR technology provides us with tools to systematically measure the functional contribution of each viral gene and to identify the host factors involved in productive infection (7). Here, we present systematic screens for both host and viral factors affecting HCMV infection in primary human fibroblasts. To capture the complexity of the molecular events during infection, we recorded the transcriptomes of tens of thousands of single cells, monitoring how perturbation of critical host and viral factors alters the timing, course, and progression of infection. Our data paint an unprecedented picture of the HCMV life cycle and its vulnerabilities to antiviral intervention.

High resolution functional landscape of the HCMV genome

It was recently shown that targeting individual essential herpesvirus genes by CRISPR/Cas9 disrupts their expression directly and their function through errors introduced by the host DNA repair machinery (8). Cleavage of the viral DNA in non-essential regions has a moderate impact on genes proximal to the cut site, but minimal impact on HCMV replication and host cell viability, likely because DNA repair is fast relative to the kinetics of replication ((8) and our data below). Thus, Cas9 represents an effective tool for making targeted disruptions in the viral genome. To enable high-resolution scanning of viral elements for a comprehensive functional annotation of the HCMV genome, we designed a single-guide RNA (sgRNA) library that targets every protospacer-adjacent motif (PAM) for *S. pyogenes* Cas9 (NGG PAM sequence present roughly every 8 bp) along the genome of the clinical HCMV strain Merlin (Fig. 1A, Table S1). We delivered the library into primary human foreskin fibroblasts engineered to express Cas9, so that upon HCMV infection, each cell executes a cut at a defined position along the viral genome, collectively tiling its entirety.

We mapped the phenotypic landscape by quantifying the abundances of individual sgRNA cassettes in cells surviving infection relative to the initial population by deep sequencing (Fig. S1). We found that cutting phenotypes are relatively constant within individual genes, i.e. the determining factor is which gene is targeted by Cas9, more so than the relative position of the target site within the gene. Adjacent sets of genes also frequently had similar phenotypes. However, some gene boundaries were marked by abrupt phenotype changes, arguing that here, strong functional consequences of Cas9-induced double-strand breaks are limited to the immediate vicinity of the cut sites (Figs. 1B, S2, Table S1).

At a larger scale, changes in the direction and magnitude of the phenotypes defined six major genomic modules: Cuts in both distal regions of the genome, which lack genes essential for viral replication (9, 10), had minimal impact on host cell survival. As expected, targeting the two regions covering UL48A–UL73 and UL96–UL150, both of which contain essential genes involved in viral DNA replication, packaging and nuclear egress (9, 11), strongly protected infected cells from death. Surprisingly, in the two remaining regions of the genome, we found that disruption of genes required for viral replication did not necessarily protect the host from death. Cuts within the UL32–UL47 region, which contains essential genes, led to a strongly increased ability of the virus to kill cells. The most strongly sensitizing phenotypes mapped to the known viral apoptosis inhibitors UL36, UL37, and UL38 (12). While this behavior can be rationalized for virally

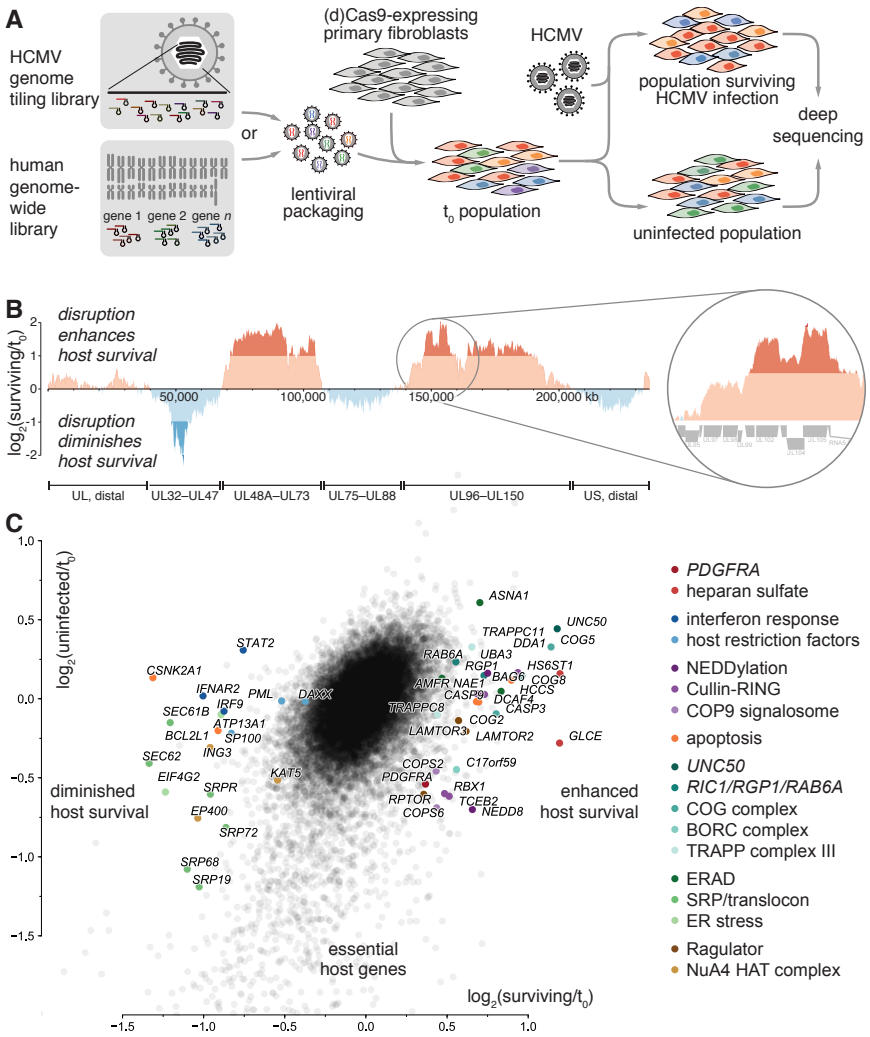

Fig. 1. Virus and host-directed CRISPR screens map the phenotypic landscape of HCMV and its host's dependency and restriction factors. (**A**) Experimental design for pooled, virus and host-directed CRISPR screening. Our HCMV tiling library or genome-wide human sgRNA libraries were lentivirally delivered into primary human foreskin fibroblasts expressing the CRISPRi or CRISPRn machinery, followed by infection with HCMV. sgRNA cassettes were quantified by deep sequencing in the initial (t_0) population, the surviving population, and the uninfected control population. (**B**) Phenotypic landscape of the HCMV genome obtained by locally averaging the phenotypes of individual sgRNAs. Strong changes in the magnitude of the phenotype coincide with gene-gene boundaries (inset). (**C**) Results of host-directed CRISPRi screen displayed as a scatter plot of average gene essentiality (i.e. infection-independent phenotype; y-axis) vs. protection/sensitization to death upon HCMV infection (i.e. infection-dependent phenotype; x-axis).

encoded anti-apoptotic proteins, it extended to many other virus-essential genes without known anti-apoptotic roles, including the DNA polymerase processivity factor UL44. Similarly, cuts in the central region spanning UL75–UL88 led to slightly enhanced host cell death upon infection. Many genes in this region are encoding essential structural components of the viral envelope, tegument, and capsid.

Targeting essential viral genes, by definition, undermines the production of viral offspring. The outcome for the host, however, is more nuanced and sometimes counterintuitive. It appears that disrupting essential genes involved in viral DNA replication mostly protects the host. However, interfering with the later steps of assembling new virions may not only be ineffective for protecting the host, but even place an additional burden, leading to enhanced host cell death.

Genome-wide screen for host factors of HCMV infection

Next, we carried out a screen for host factors modulating HCMV infection by systematically repressing expression of human genes by CRISPR interference (CRISPRi) (13, 14). Phenotypes were defined by enrichment or depletion of sgRNA cassettes in the surviving cell population over the initial population, as well as in an uninfected control population to account for host gene essentiality (Fig. 1C, Table S2).

Our screen revealed a range of diverse host genes required for multiple steps in the viral life cycle. Genes involved in the biosynthesis of heparan sulfate were among the strongest protective hits. Heparan sulfate proteoglycans on the cell surface enable the adhesion of HCMV prior to cell entry (15, 16). Additionally, we found a range of vesicle trafficking factors: RAB6A and its GEFs RIC1/KIAA1432 and RGP1, the conserved oligomeric Golgi (COG) complex, members of TRAPP complex III, and UNC50. These factors converge on the Golgi apparatus and mediate both retrograde and anterograde transport, implying that they act downstream of viral entry. Some had previously been implicated in the internalization of diverse bacterial and plant toxins, suggesting that HCMV and toxins exploit similar pathways for cell entry (13, 17–21). Other protective hits included members of the LAMTOR/Ragulator complex, Folliculin (FLCN), and the Lyspersin (C17orf59) subunit of the BORC complex, all linked to lysosome positioning and nutrient sensing (22–24). This supports and extends the recent observation that HCMV infection changes lysosome dynamics (6). Addition-

ally, host cell death was reduced by knockdown of certain Cullin-RING E3 ligases, adaptor subunits, substrate receptors, regulators, and the associated neddylation and deneddylation machineries. Many viruses, including HCMV, hijack this pathway to degrade host restriction factors, which can be prevented by broadly-acting NEDD8-activating enzyme inhibitors (25, 26). Finally, we identified genes involved in tail-anchored protein insertion into the ER, as well as ER-associated degradation: *AMFR*, an E3 ligase, and the TRC40/GET pathway members *BAG6* and *ASNA1*, which were shown to be required for insertion of membrane proteins of herpes simplex virus I which, however, lack HCMV orthologs (27).

Our screens also identified a number of host factors whose knockdown sensitizes cells to death upon infection rather than protecting them. Among these were known restriction factors such as *PML* and *DAXX*, as well as members of the interferon type I (IFN) pathway. We also found subunits of the NuA4 histone acetyltransferase complex, which was shown to counteract Hepatitis-B virus (28). Other sensitizing hits included members of the signal recognition particle, the translocon and associated factors, and genes involved in ER stress (29, 30). Finally, we found genes with anti-apoptotic function, whose removal likely increases the sensitivity to apoptosis triggered by HCMV infection.

To validate and extend the host factors identified in the CRISPRi screen, we conducted a knockout screen using an established CRISPR cutting (CRISPRn) library (31) (Fig. S3A, Table S2). The CRISPRi and CRISPRn screens were in general agreement (Fig. S3B). However, the phenotypes of hits involved in virus entry, as well as pro- and anti-apoptotic genes, were more pronounced in the knockout screen, consistent with the notion that selection pressure acts more strongly on cells with true null alleles compared to cells with residual expression of targeted genes. *PDGFRA* stood out as the top protective hit, supporting its described role as HCMV entry receptor in fibroblasts (32–35). Conversely, genes that are essential for host viability and factors with weaker phenotypes were often not enriched above background in the CRISPRn screen. One reason may be the toxicity of DNA cutting *per se*, especially in a cell type with an intact p53 response (36, 37). Our findings underscore the benefits of combining orthogonal modes of genetic screening (38).

The lytic cascade resolved by single-cell transcriptomics

Our pooled screens provide a genome-scale picture of the factors involved in lytic HCMV infection. To investigate the roles of critical host and viral factors in more detail, we used Perturb-seq, which combines CRISPR-based genetic perturbations with a rich transcriptional readout at the single-cell level (29, 39–41). Measuring tens of thousands of single-cell transcriptomes provides a massively parallel way of testing large numbers of genetic perturbations under controlled conditions with a high-dimensional readout. The single-cell nature of this approach makes it particularly well suited for studying virus infection, a process with great inherent variability from cell to cell (42–46).

To lay the groundwork for the Perturb-seq analysis, we explored the spectrum of cellular states in response to infection by recording single-cell transcriptomes from cells sampled from eight time points with two multiplicities of infection each (Fig. 2A). Instead of synchronizing cells experimentally, which has inherent limits to its resolution due to intrinsic heterogeneity in the timing at which individual cells are infected and the rate of progression of the infection, we staged cells computationally by their transcriptional signatures. The largest sources of variability between cells were the extent of IFN signaling and the viral load, i.e. the fraction of viral transcripts per cell, which reached levels of around 75 % and was positively correlated with total cellular RNA content (Fig. S4). Together, these properties define three main subpopulations of cells: a naïve population (uninfected and IFN-negative); a bystander population (uninfected and IFN-positive); and an infected population with varying amounts of viral transcripts (Fig. 2B). Of note, while activation of IFN-stimulated genes (ISGs) and early viral gene expression happen at the same experimental time points, they are almost entirely segregated to different populations of cells, and only a small cohort of cells with low viral loads also express ISGs. This phenomenon may present itself as an apparent correlation of some viral genes with ISGs in bulk measurements, but has been described in single-cell studies of herpes simplex virus 1 (4, 45). Together, this underscores the rapidity with which the virus actively suppresses IFN signaling (see S4B).

When looking at viral gene expression, we found that after an initial noisy phase, the majority of infected cells followed a dominant and highly stereotypical trajectory with increasing viral load. A subpopulation of around 2 % of cells, however, followed an alternate trajectory (Fig. 2C). Staging cells *in silico* for each trajectory enabled us to calculate high-resolution expression patterns of individual viral genes as a function of a 'pseudo-temporal' axis defined by viral load. Hierarchical clustering of individual viral transcripts along the dominant trajectory broadly recapitulated the established classes of 'immediate-early', 'delayed-early', 'leaky-late' and 'true-late' genes, but with a high degree of pseudo-temporal fine structure within each class (Fig. 2D, S5) thus providing a far higher resolution view of these waves. In agreement with the classification based on proteomics measurements (4), we defined an additional 'intermediate' kinetic pattern.

The alternate trajectory, followed by $\sim$2 % of cells, was characterized by a uniform increase of early genes, an almost complete absence of true-late transcripts and of the otherwise abundant major non-coding RNAs and generally low total cellular RNA content, indicating that this trajectory is abortive (Figs. 2E, S5). The pattern of expressed genes showed no enrichment of specific genomic loci, arguing against the hypothesis that this subpopulation might be infected by virions with defined long-range genomic defects (Fig. S5).

Focusing on the patterns of host gene expression as a function of viral load, we found that once interferon signaling

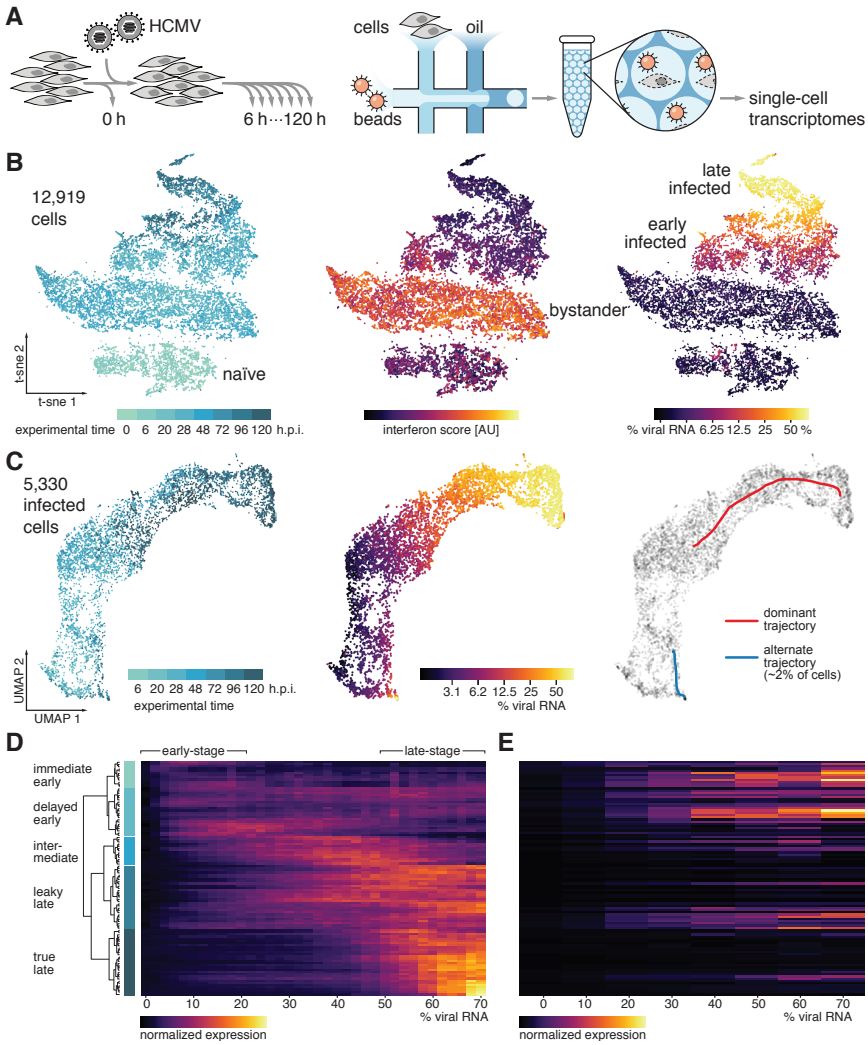

Fig. 2. Single-cell infection time-course defines the lytic cascade of expression events as a trajectory in viral gene expression space. (**A**) Cells were infected with a low or high MOI of HCMV, harvested after times ranging from 6–120 h.p.i., pooled and subjected to emulsion-based single-cell RNA-seq. (**B**) t-sne projection of all 12,919 cells color-coded by experimental time point (left), interferon activation score (center), or viral load (right) defining the naïve, bystander, and infected subpopulations. (**C**) UMAP projection of the viral parts of the transcriptomes of 5,330 infected cells (>2.5 % viral load; >5 % for time points ⩾72 h.p.i), color-coded by experimental time (left) or viral load (center). Trajectories were determined by averaging the position of cells ranked by viral load. (**D**) Clustering of averaged viral gene expression in cells binned in increments of 2 % by viral load recapitulates the temporal waves of genes in the lytic cascade. (**E**) The same cluster order applied on the viral gene expression pattern along the alternate trajectory, binned in increments of 10 %. For higher resolution see Fig. S5).

is halted in early-infected cells, most host transcripts behave coherently as viral load increases (Fig. S6). HCMV, unlike other herpesviruses, is known to allow translation of host transcripts to proceed selectively (47). Some housekeeping transcripts (e.g. those of ribosomal proteins) decreased in abundance, suggesting that they are being actively suppressed (48, 49). A small but prominent set of host transcripts were upregulated, including CD55, which was previously seen at the protein level (4) and shown to be incorporated into budding virions to counteract the complement system (50).

Only cells in the G1 phase of the cell cycle are permissive to the progression of infection (51). Accordingly, we observed that G1 cells are gradually depleted from the population of uninfected cells, and a majority of infected cells adopt a G1-like state (Fig. S7A, B). Most cells later abruptly switched to a state most resembling S-phase. This transition co-occurs with the onset of 'true-late' gene expression, which marks the beginning of viral genome replication (see Fig. S5B) and likely reflects the pseudo-mitotic state described for cells in late-stage infection (52).

Host and virus-directed genetic perturbations lead to conceptually different outcomes

We next conducted a series of Perturb-seq experiments exploring the impact of targeting either host or viral factors on the viral replication cycle. In contrast to the pooled screen, where phenotypes emerge by enrichment or depletion of cells over multiple days, Perturb-seq provides a high-resolution view of the impact of targeting a viral or host gene over the ∼72 h course of a single viral replication cycle.

We first selected 52 host genes with protective or sensitizing phenotypes identified in the pooled screens (Fig. 3A, B, Table S3). We monitored how perturbing them by CRISPRi changes the host cell transcriptomes and the propensity of cells to get infected when challenged with HCMV at a low multiplicity of infection (MOI) (Fig. 3C, D). In uninfected cell populations, we observed the strongest transcriptional responses with knockdown of LAMTOR/Ragulator subunits and the neddylation machinery, as well as mild responses to the knockdowns of vesicle trafficking factors, and of genes associated with the translocon. The patterns of the transcriptional responses to the knockdowns organized host factors by biological pathway in a principled fashion (Fig. 3C). This required no prior knowledge and provided a layer of informa-

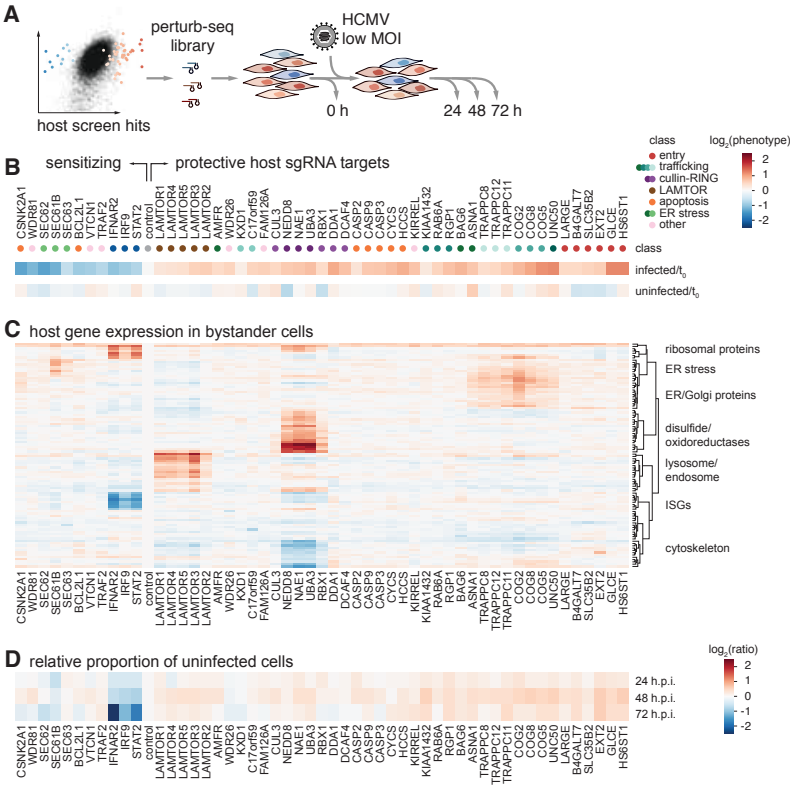

Fig. 3. Transcriptional responses to host factor knockdowns. (**A**) Host dependency and restriction factors were selected from the pooled screen, cloned into a Perturb-seq library, delivered into dCas9-expressing fibroblasts, which were challenged with a low MOI of HCMV for 24–72 h. (**B**) Selected host factors have a wide range of sensitizing to protective phenotypes, varying degrees of essentiality and cover different pathways. (**C**) Transcriptional response to host gene perturbations, shown as a set of the most responsive host genes, relative to control cells in the bystander population (here defined as cells with <1 % viral load from the 24–72 h.p.i. time points). See also Fig. S8. (**D**) Fraction of cells that remained uninfected (<1 % viral RNA) at 24, 48 and 72 h.p.i., displayed as ratio relative to the cell population expressing control sgRNAs.

tion that would have remained unresolved when ranking hits simply by their phenotypes in the pooled screens. The transcriptional patterns were mostly similar in naïve cells compared to the bystander population, however, knockdown of IFN pathway members prevented cells from mounting the response characteristic of bystander cells (Fig. S8).

The Perturb-seq data also revealed the proportion of cells that remained uninfected after HCMV challenge (Fig. 3D). The results correlated broadly with the low-resolution view obtained in the pooled screen; for example, knockdown of interferon pathway members led to a strong increase in the numbers of infected cells.

In order to follow changes in viral gene expression in infected cells, we next carried out a Perturb-seq experiment where we challenged cells with a high MOI of HCMV. We used CRISPRn, allowing us to target viral genes in addition to host factors. Based on their strongly protective or sensitizing phenotypes in the pooled, virus-directed screen, we selected 31 viral gene targets, in addition to a representative set of 21 host factors, for which we verified that knockdown and knockout trigger comparable host responses (Fig. 4A, B, Table S3, Fig. S9).

We found that the time course of progression of infection varied widely depending on the targeted gene (Fig. 4C). Control cells gradually transitioned from being predominantly early-stage to predominantly late-stage. Perturbation of host factors caused shifts in this bimodal distribution (Fig. 4C, left panel). For example, knockout of *PDGFRA* (the proposed viral receptor (33)) or *HS6ST1* (involved in heparan sulfate biosynthesis) prevented any accumulation of viral transcripts. Similarly, no appreciable quantities of viral transcripts were found in cells lacking *COG8* or *UNC50*, implicating these factors as novel components required for viral entry. Perturbation of Ragulator/*LAMTOR* and *FLCN*, as well as *RIC1/KIAA1432* and *RGP1*, allowed infected cells to initially progress to early-stage, but then caused a stall. This suggests these factors act downstream of viral uncoating but prior to viral genome replication. Conversely, blocking the interferon pathway caused an acceleration of progression, with most cells reaching late-stage prematurely, at 48 h post-infection. Finally, knockout of pro/anti-apoptotic host genes, among others, barely changed the viral load distribution compared to the negative controls, suggesting that rather than impacting the course of infection itself, these interfere with the ability of the virus to kill the cells in a way that is not immediately apparent at the transcript level.

Compared to targeting host genes, targeting viral genes typically led to qualitatively different outcomes. The distributions of viral loads were no longer bimodal, but multimodal (Fig. 4C, right panel), prompting us to monitor the underlying patterns of individual viral genes, rather than looking at viral genes in aggregate by way of the viral load (Fig. 4D). In the space of viral gene expression, all trajectories defined by cells with perturbed host genes were nearly congruent with the control trajectories, indicating that host genes do not determine the patterns of viral gene expression at the different stages of infection (Fig. 4D, top). Rather, host-directed perturbations determine which stage of infection can be reached and how quickly. In marked contrast, when we targeted viral genes, infection progressed along radically distinct trajectories in expression space that diverge from the default and fall into a set of classes (Fig. 4D, bottom). Cells with

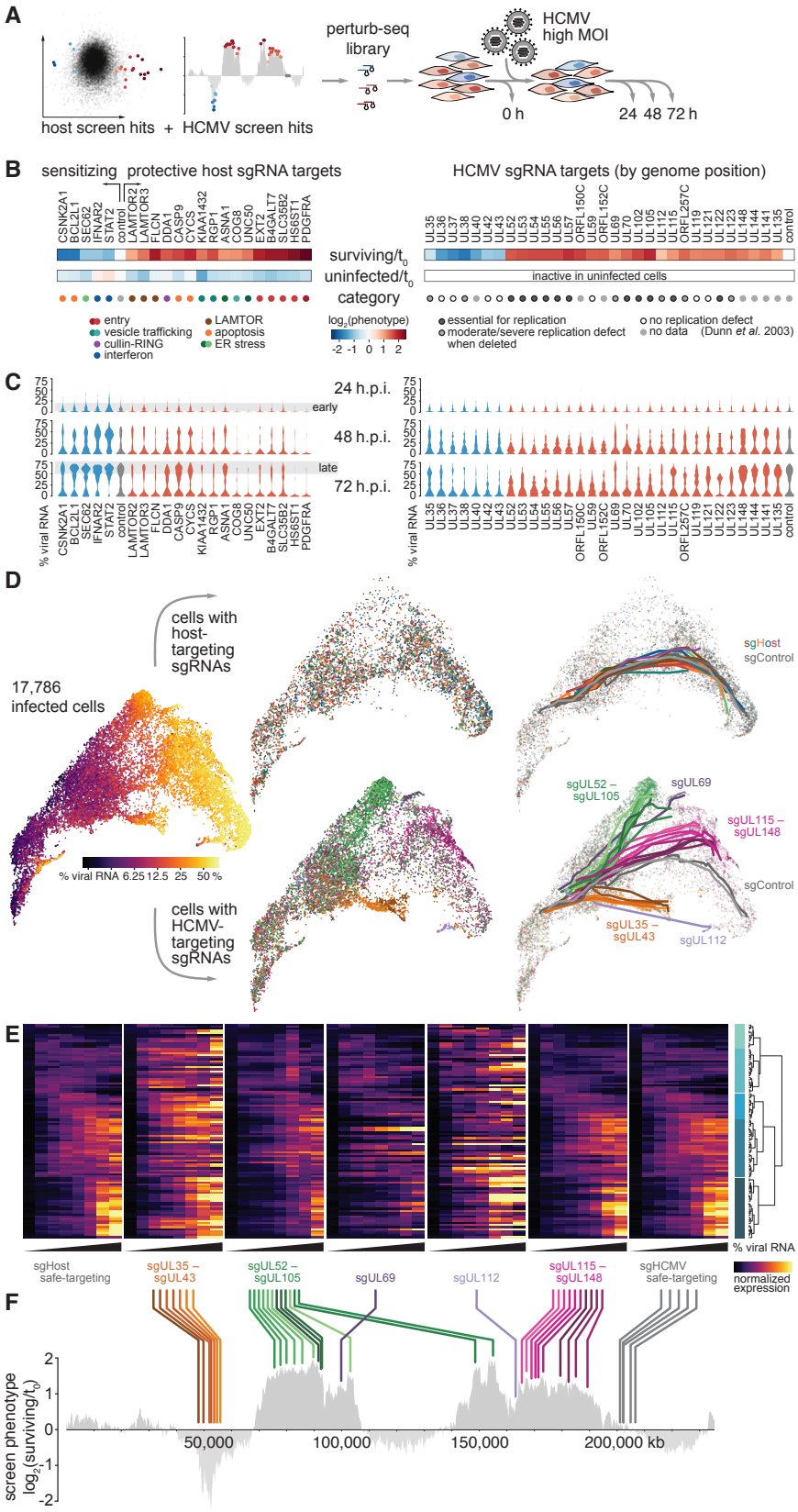

Fig. 4. Host and virus-directed perturbations stall or accelerate progression, or create alternate trajectories in viral gene expression space. (**A**) Host and viral factors were selected from the pooled screens, cloned into a Perturb-seq library, delivered into Cas9-expressing fibroblasts, which were challenged with a high MOI of HCMV for 24–72 h. (**B**) Selected factors organized by their respective phenotypes in the pooled screens, essentiality for the host and the virus (9), respectively, and pathway membership. (**C**) Violin plots of viral loads as a function of time after infection and the perturbed factor (red, protective phenotype; blue, sensitizing phenotype; grey, control) (**D**) UMAP projection of the viral parts of the transcriptomes of infected cells, color-coded by viral load. Subset of cells with host-directed (top) or virus-directed (bottom) sgRNAs, color-coded by guide identity. Trajectories were determined by averaging the geometric position of cells with a given sgRNA, ranked by viral load. (**E**) Averaged viral gene expression profiles along the groups of trajectories, determined from cells binned by viral load. (**F**) Perturbed viral genes from each trajectory set, mapped back to their respective positions in the HCMV genome.

sgRNAs targeting non-essential regions of the viral genome followed the same trajectory as those with host-targeting controls, showing only mild transcriptional effects on genes in the vicinity of the cut sites (Figs. S10, S11).

Alternate trajectories were arranged in three main bundles (Fig. 4E, F): The first class of trajectories was established by targeting genes in the strongly sensitizing region (UL35–UL43). Here, the number of cells declined rapidly with increased viral load, in agreement with the higher susceptibility to cell death upon infection found in the pilot screen (Fig. S10). In addition to creating a pro-apoptotic state, a surprising feature of these alternate trajectories was the failure to shut down expression of immediate-early and delayed-early genes once later stage genes were expressed (Fig. 4F). A second bundle corresponded to perturbations of genes in the first strongly protective module (UL52–ORFL152C), as well as UL102 and UL105. These trajectories showed a marked delay and reduced induction of true-late genes, with few cells reaching high viral loads, indicating a failure to replicate the viral genome. A third bundle contained perturbations of genes located within the UL115–UL148 region. This bundle was most similar to the unperturbed trajectories. Of note, the kinetics of progression varied between the targeted genes within this group (Fig. 4C, right), with perturbation of the major immediate-early transactivator genes UL122 and UL123 causing the strongest delays. Finally, cells with perturbations of UL69 and UL112, genes with comparatively weak protective phenotypes, defined two trajectories distinct from the three main bundles, despite their genome positions adjacent to or within genes belonging to the main bundles (Fig. 4F). Targeting UL69 caused overexpression of RNA1.2, while targeting of UL112 triggered widespread deregulation of genes from all temporal classes (Figs. 4E, S10). Taken together, this shows that adherence to the normal viral trajectory is orchestrated by a diversity of viral genes, but not host factors.

Discussion

The waves of viral gene expression during lytic infection are a key signature of herpesvirus biology and its molecular players are subjects of intense investigation (53). Here, we introduce a functional single-cell genomics approach to study lytic HCMV infection with unprecedented temporal and gene expression resolution. We combine comprehensive pooled CRISPR screening, directed against both host and virus, with massively parallel single-cell transcriptional analysis of infection. Together, this strategy identifies genes critical for infection and pinpoints their specific roles by observing the changes in the course of infection when each factor is perturbed.

Our study redefines the lytic cascade at the single-cell level as a highly resolved continuum of cellular states, which would otherwise be obscured by differences in the kinetics of infection in bulk experiments. We find that the large majority of cells follow this stereotypical trajectory in viral gene expression space, while a small but prominent subpopulation take an alternate, abortive trajectory.

Most importantly, we reveal a dichotomy in how the system reacts to host- versus virus-directed perturbations: Targeting critical host factors alters how fast or how far cells can progress along the lytic cascade. If the lack of a factor stalls progression, this directly reveals the phase at which this factor plays a critical role. Conversely, targeting viral factors can alter the course of infection by creating defined and specific alternate trajectories that do not necessarily culminate in successful replication or that drive cells into premature apoptosis. This dichotomy, may be a general feature of virus-host systems. HCMV is entirely dependent on the transcriptional and translational machinery of its host. At the same time, our findings indicate that the lytic cascade is a deterministic program, which, once set in motion, is solely controlled by viral factors.

Our work also provides a roadmap for the design of effective antiviral combination therapies by selecting sets of targets that drive the virus into distinct, nonproductive pathways while sparing or inducing apoptosis in the host, depending on the desired outcome. Similarly, our data can inform the design of engineered attenuated viral strains for vaccine development purposes. More generally, we envision that our approach can serve as a blueprint for studying other viruses and to define their vulnerabilities to genetic or pharmacological interventions.

ACKNOWLEDGMENTS

We thank M. A. Horlbeck for designing the HCMV tiling library, L. A. Gilbert for help setting up pooled screens, T. M. Norman, M. A. Horlbeck, J. A. Hussmann and X. Qiu for help with data analysis. A. Xu, J. A. Villalta and R. A. Pak provided technical assistance. The UCOE sequence was a gift from G. Sienski. We thank T. Fair for help with Perturb-seq experiments. We thank N. Stern-Ginossar, M. J. Shurtleff, M. Jost, R. A. Saunders and all members of the Weissman lab for insightful discussions. J. Winkler and A. S. Puschnik provided helpful comments on the manuscript. Special thanks to O. Wueseke (impulse-science.org) for editorial help. *Funding:* J.S.W. is a Howard Hughes Medical Institute Investigator. M.Y.H. was supported by an EMBO long-term postdoctoral fellowship (EMBO ALTF 1193-2015, co-funded by the European Commission FP7, Marie Curie Actions, LTFCOFUND2013, GA-2013-609409). *Author contributions:* M.Y.H. and J.S.W. conceptualized the study, interpreted the experiments and wrote the manuscript. M.Y.H. designed and carried out the experiments. *Competing Interests:* J.S.W. and M.Y.H. have filed patent applications related to CRISPRi screening and Perturb-seq. J.S.W. consults for and holds equity in KSQ Therapeutics and Maze Therapeutics, and consults for 5AM Ventures. *Data and materials availability:* Plasmids and libraries will be made available via addgene. Raw sequencing data will be deposited to GEO.

References

1. Derek Gatherer, Sepehr Seirafian, Charles Cunningham, Mary Holton, Derrick J Dargan, Katarina Baluchova, Ralph D Hector, Julie Galbraith, Pawel Herzyk, Gavin W G Wilkinson, and Andrew J Davison. High-resolution human cytomegalovirus transcriptome. *Proc. Natl. Acad. Sci. U. S. A.*, 108(49):19755–19760, December 2011.
2. Lisa Marcinowski, Michael Lidschreiber, Lukas Windhager, Martina Rieder, Jens B Bosse, Bernd Rädle, Thomas Bonfert, Ildiko Györy, Miranda de Graaf, Olivia Prazeres da Costa, Philip Rosenstiel, Caroline C Friedel, Ralf Zimmer, Zsolt Ruzsics, and Lars Dölken. Real-time transcriptional profiling of cellular and viral gene expression during lytic cytomegalovirus infection. *PLoS Pathog.*, 8(9):e1002908, September 2012.
3. Noam Stern-Ginossar, Ben Weisburd, Annette Michalski, Vu Thuy Khanh Le, Marco Y Hein, Sheng-Xiong Huang, Ming Ma, Ben Shen, Shu-Bing Qian, Hartmut Hengel, Matthias Mann, Nicholas T Ingolia, and Jonathan S Weissman. Decoding human cytomegalovirus. *Science*, 338(6110):1088–1093, November 2012.
4. Michael P Weekes, Peter Tomasec, Edward L Huttlin, Ceri A Fielding, David Nusinow, Richard J Stanton, Eddie C Y Wang, Rebecca Aicheler, Isa Murrell, Gavin W G Wilkinson, Paul J Lehner, and Steven P Gygi. Quantitative temporal viromics: an approach to investigate host-pathogen interaction. *Cell*, 157(6):1460–1472, June 2014.
5. Osnat Tirosh, Yifat Cohen, Alina Shitrit, Odem Shani, Vu Thuy Khanh Le-Trilling, Mirko Trilling, Gilgi Friedlander, Marvin Tanenbaum, and Noam Stern-Ginossar. The transcription and translation landscapes during human cytomegalovirus infection reveal novel Host-Pathogen interactions. *PLoS Pathog.*, 11(11):e1005288, November 2015.
6. Pierre M Jean Beltran, Rommel A Mathias, and Ileana M Cristea. A portrait of the human organelle proteome in space and time during cytomegalovirus infection. *Cell Syst*, 3(4): 361–373.e6, October 2016.

7. Andreas S Puschnik, Karim Majzoub, Yaw Shin Ooi, and Jan E Carette. A CRISPR toolbox to study virus-host interactions. *Nat. Rev. Microbiol.*, 15(6):351–364, June 2017.
8. Ferdy R van Diemen, Elisabeth M Kruse, Marjolein J G Hooykaas, Carlijn E Bruggeling, Anita C Schürch, Petra M van Ham, Saskia M Imhof, Monique Nijhuis, Emmanuel J H J Wiertz, and Robert Jan Lebbink. CRISPR/Cas9-Mediated genome editing of herpesviruses limits productive and latent infections. *PLoS Pathog.*, 12(6):e1005701, June 2016.
9. Walter Dunn, Cassie Chou, Hong Li, Rong Hai, David Patterson, Viktor Stolc, Hua Zhu, and Fenyong Liu. Functional profiling of a human cytomegalovirus genome. *Proc. Natl. Acad. Sci. U. S. A.*, 100(24):14223–14228, November 2003.
10. Dong Yu, Maria C Silva, and Thomas Shenk. Functional map of human cytomegalovirus AD169 defined by global mutational analysis. *Proc. Natl. Acad. Sci. U. S. A.*, 100(21): 12396–12401, October 2003.
11. Ellen Van Damme and Marnix Van Loock. Functional annotation of human cytomegalovirus gene products: an update. *Front. Microbiol.*, 5:218, May 2014.
12. A Louise McCormick, Anna Skaletskaya, Peter A Barry, Edward S Mocarski, and Victor S Goldmacher. Differential function and expression of the viral inhibitor of caspase 8-induced apoptosis (vICA) and the viral mitochondria-localized inhibitor of apoptosis (vMIA) cell death suppressors conserved in primate and rodent cytomegaloviruses. *Virology*, 316(2):221–233, November 2003.
13. Luke A Gilbert, Max A Horlbeck, Britt Adamson, Jacqueline E Villalta, Yuwen Chen, Evan H Whitehead, Carla Guimaraes, Barbara Panning, Hidde L Ploegh, Michael C Bassik, Lei S Qi, Martin Kampmann, and Jonathan S Weissman. Genome-Scale CRISPR-Mediated control of gene repression and activation. *Cell*, 159(3):647–661, October 2014.
14. Max A Horlbeck, Luke A Gilbert, Jacqueline E Villalta, Britt Adamson, Ryan A Pak, Yuwen Chen, Alexander P Fields, Chong Yon Park, Jacob E Corn, Martin Kampmann, and Jonathan S Weissman. Compact and highly active next-generation libraries for CRISPR-mediated gene repression and activation. *Elife*, 5, September 2016.
15. T Compton, D M Nowlin, and N R Cooper. Initiation of human cytomegalovirus infection requires initial interaction with cell surface heparan sulfate. *Virology*, 193(2):834–841, April 1993.
16. Stefanie Hetzenecker, Ari Helenius, and Magdalena Anna Krzyzaniak. HCMV induces macropinocytosis for host cell entry in fibroblasts. *Traffic*, 17(4):351–368, April 2016.
17. Ganesh V Pusapati, Giovanni Luchetti, and Suzanne R Pfeffer. Ric1-Rgp1 complex is a guanine nucleotide exchange factor for the late golgi Rab6A GTPase and an effector of the medial golgi Rab33B GTPase. *Journal of Biological Chemistry*, 287(50):42129–42137, 2012.
18. Richard D Smith, Rose Willett, Tetyana Kudlyk, Irina Pokrovskaya, Adrienne W Paton, James C Paton, and Vladimir V Lupashin. The COG complex, rab6 and COPI define a novel golgi retrograde trafficking pathway that is exploited by SubAB toxin. *Traffic*, 10(10): 1502–1517, October 2009.
19. Sicen Liu, Monika Dominska-Ngowe, and Derek Michael Dykxhoorn. Target silencing of components of the conserved oligomeric golgi complex impairs HIV-1 replication. *Virus Res.*, 192:92–102, November 2014.
20. Michael C Bassik, Martin Kampmann, Robert Jan Lebbink, Shuyi Wang, Marco Y Hein, Ina Poser, Jimena Weibezahn, Max A Horlbeck, Siyuan Chen, Matthias Mann, Anthony A Hyman, Emily M LeProust, Michael T McManus, and Jonathan S Weissman. A systematic mammalian genetic interaction map reveals pathways underlying ricin susceptibility. *Cell*, 152(4):909–922, 2013.
21. Andrey S Selyunin, Lakesla R Iles, Geoffrey Bartholomeusz, and Somshuvra Mukhopadhyay. Genome-wide siRNA screen identifies UNC50 as a regulator of shiga toxin 2 trafficking. *J. Cell Biol.*, 216(10):3249–3262, October 2017.
22. Georgina P Starling, Yan Y Yip, Anneri Sanger, Penny E Morton, Emily R Eden, and Mark P Dodding. Folliculin directs the formation of a Rab34-RILP complex to control the nutrient-dependent dynamic distribution of lysosomes. *EMBO Rep.*, 17(6):823–841, June 2016.
23. Przemyslaw A Filipek, Mariana E G de Araujo, Georg F Vogel, Cedric H De Smet, Daniela Eberharter, Manuele Rebsamen, Elena L Rudashevskaya, Leopold Kremser, Teodor Yordanov, Philipp Tschaikner, Barbara G Fürnrohr, Stefan Lechner, Theresia Dunzendorfer-Matt, Klaus Scheffzek, Keiryn L Bennett, Giulio Superti-Furga, Herbert H Lindner, Taras Stasyk, and Lukas A Huber. LAMTOR/Ragulator is a negative regulator of arl8b- and BORC-dependent late endosomal positioning. *J. Cell Biol.*, 216(12):4199–4215, December 2017.
24. Jing Pu, Tal Keren-Kaplan, and Juan S Bonifacino. A Ragulator-BORC interaction controls lysosome positioning in response to amino acid availability. *J. Cell Biol.*, 216(12):4183–4197, December 2017.
25. Tanja Becker, Vu Thuy Khanh Le-Trilling, and Mirko Trilling. Cellular cullin RING ubiquitin ligases: Druggable host dependency factors of cytomegaloviruses. *Int. J. Mol. Sci.*, 20(7), April 2019.
26. Vu Thuy Khanh Le-Trilling, Dominik A Megger, Benjamin Katschinski, Christine D Landsberg, Meike U Rückborn, Sha Tao, Adalbert Krawczyk, Wibke Bayer, Ingo Drexler, Matthias Tenbusch, Barbara Sitek, and Mirko Trilling. Broad and potent antiviral activity of the NAE inhibitor MLN4924. *Sci. Rep.*, 6:19977, February 2016.
27. Melanie Ott, Débora Marques, Christina Funk, and Susanne M Bailer. Asna1/TRC40 that mediates membrane insertion of tail-anchored proteins is required for efficient release of herpes simplex virus 1 virions. *Virol. J.*, 13(1):175, October 2016.
28. Hironori Nishitsuji, Saneyuki Ujino, Keisuke Harada, and Kunitada Shimotohno. TIP60 complex inhibits hepatitis B virus transcription. *J. Virol.*, 92(6), March 2018.
29. Britt Adamson, Thomas M Norman, Marco Jost, Min Y Cho, James K Nuñez, Yuwen Chen, Jacqueline E Villalta, Luke A Gilbert, Max A Horlbeck, Marco Y Hein, Ryan A Pak, Andrew N Gray, Carol A Gross, Atray Dixit, Oren Parnas, Aviv Regev, and Jonathan S Weissman. A multiplexed Single-Cell CRISPR screening platform enables systematic dissection of the unfolded protein response. *Cell*, 167(7):1867–1882.e21, December 2016.
30. Yifat Cohen, Márton Megyeri, Oscar C W Chen, Giuseppe Condomitti, Isabelle Riezman, Ursula Loizides-Mangold, Alaa Abdul-Sada, Nitzan Rimon, Howard Riezman, Frances M Platt, Anthony H Futerman, and Maya Schuldiner. The yeast p5 type ATPase, spf1, regulates manganese transport into the endoplasmic reticulum. *PLoS One*, 8(12):e85519, December 2013.
31. Konstantinos Tzelepis, Hiroko Koike-Yusa, Etienne De Braekeleer, Yilong Li, Emmanouil Metzakopian, Oliver M Dovey, Annalisa Mupo, Vera Grinkevich, Meng Li, Milena Mazan, Malgorzata Gozdecka, Shuhei Ohnishi, Jonathan Cooper, Miten Patel, Thomas McKerrell, Bin Chen, Ana Filipa Domingues, Paolo Gallipoli, Sarah Teichmann, Hannes Ponstingl, Ultan McDermott, Julio Saez-Rodriguez, Brian J P Huntly, Francesco Iorio, Cristina Pina, George S Vassiliou, and Kosuke Yusa. A CRISPR dropout screen identifies genetic vulnerabilities and therapeutic targets in acute myeloid leukemia. *Cell Rep.*, 17(4):1193–1205, October 2016.
32. Liliana Soroceanu, Armin Akhavan, and Charles S Cobbs. Platelet-derived growth factor-α receptor activation is required for human cytomegalovirus infection. *Nature*, 455(7211): 391–395, 2008.
33. Anna Kabanova, Jessica Marcandalli, Tongqing Zhou, Siro Bianchi, Ulrich Baxa, Yaroslav Tsybovsky, Daniele Lilleri, Chiara Silacci-Fregni, Mathilde Foglierini, Blanca Maria Fernandez-Rodriguez, Aliaksandr Druz, Baoshan Zhang, Roger Geiger, Massimiliano Pagani, Federica Sallusto, Peter D Kwong, Davide Corti, Antonio Lanzavecchia, and Laurent Perez. Platelet-derived growth factor-α receptor is the cellular receptor for human cytomegalovirus gHgLgO trimer. *Nat Microbiol*, 1(8):16082, June 2016.
34. Nadia Martinez-Martin, Jessica Marcandalli, Christine S Huang, Christopher P Arthur, Michela Perotti, Mathilde Foglierini, Hoangdung Ho, Annie M Dosey, Stephanie Shriver, Jian Payandeh, Alexander Leitner, Antonio Lanzavecchia, Laurent Perez, and Claudio Ciferri. An unbiased screen for human cytomegalovirus identifies neuropilin-2 as a central viral receptor. *Cell*, July 2018.
35. Xiaofei E, Paul Meraner, Ping Lu, Jill M Perreira, Aaron M Aker, William M McDougall, Ronghua Zhuge, Gary C Chan, Rachel M Gerstein, Patrizia Caposio, Andrew D Yurochko, Abraham L Brass, and Timothy F Kowalik. OR14I1 is a receptor for the human cytomegalovirus pentameric complex and defines viral epithelial cell tropism. *Proc. Natl. Acad. Sci. U. S. A.*, 116(14):7043–7052, April 2019.
36. Tim Wang, Kıvanç Birsoy, Nicholas W Hughes, Kevin M Krupczak, Yorick Post, Jenny J Wei, Eric S Lander, and David M Sabatini. Identification and characterization of essential genes in the human genome. *Science*, 350(6264):1096–1101, November 2015.
37. Robert J Ihry, Kathleen A Worringer, Max R Salick, Elizabeth Frias, Daniel Ho, Kraig Theriault, Sravya Kommineni, Julie Chen, Marie Sondey, Chaoyang Ye, Ranjit Randhawa, Tripti Kulkarni, Zinger Yang, Gregory McAllister, Carsten Russ, John Reece-Hoyes, William Forrester, Gregory R Hoffman, Ricardo Dolmetsch, and Ajamete Kaykas. p53 inhibits CRISPR-Cas9 engineering in human pluripotent stem cells. *Nat. Med.*, 24(7):939–946, July 2018.
38. David W Morgens, Richard M Deans, Amy Li, and Michael C Bassik. Systematic comparison of CRISPR/Cas9 and RNAi screens for essential genes. *Nat. Biotechnol.*, 34(6): 634–636, June 2016.
39. Paul Datlinger, André F Rendeiro, Christian Schmidl, Thomas Krausgruber, Peter Traxler, Johanna Klughammer, Linda C Schuster, Amelie Kuchler, Donat Alpar, and Christoph Bock. Pooled CRISPR screening with single-cell transcriptome readout. *Nat. Methods*, 14(3):297–301, March 2017.
40. Atray Dixit, Oren Parnas, Biyu Li, Jenny Chen, Charles P Fulco, Livnat Jerby-Arnon, Nemanja D Marjanovic, Danielle Dionne, Tyler Burks, Raktima Raychowdhury, Britt Adamson, Thomas M Norman, Eric S Lander, Jonathan S Weissman, Nir Friedman, and Aviv Regev. Perturb-Seq: Dissecting molecular circuits with scalable Single-Cell RNA profiling of pooled genetic screens. *Cell*, 167(7):1853–1866.e17, December 2016.
41. Diego Adhemar Jaitin, Assaf Weiner, Ido Yofe, David Lara-Astiaso, Hadas Keren-Shaul, Eyal David, Tomer Meir Salame, Amos Tanay, Alexander van Oudenaarden, and Ido Amit. Dissecting immune circuits by linking CRISPR-Pooled screens with Single-Cell RNA-Seq. *Cell*, 167(7):1883–1896.e15, December 2016.
42. Fabio Zanini, Szu-Yuan Pu, Elena Bekerman, Shirit Einav, and Stephen R Quake. Single-cell transcriptional dynamics of flavivirus infection. *eLife*, 7, 2018.
43. Alistair B Russell, Cole Trapnell, and Jesse D Bloom. Extreme heterogeneity of influenza virus infection in single cells. *Elife*, 7, February 2018.
44. Florian Erhard, Marisa A P Baptista, Tobias Krammer, Thomas Hennig, Marius Lange, Panagiota Arampatzi, Christopher S Jürges, Fabian J Theis, Antoine-Emmanuel Saliba, and Lars Dölken. scSLAM-seq reveals core features of transcription dynamics in single cells. *Nature*, 571(7765):419–423, July 2019.
45. Nir Drayman, Parthiv Patel, Luke Vistain, and Savaş Tay. Hsv-1 single-cell analysis reveals the activation of anti-viral and developmental programs in distinct sub-populations. *eLife*, 8: e46339, 2019.
46. Emanuel Wyler, Vedran Franke, Jennifer Menegatti, Christine Kocks, Anastasiya Boltengagen, Samantha Praktiknjo, Barbara Walch-Rueckheim, Nikolaus Rajewsky, Friedrich Graesser, Altuna Akalin, and Markus Landthaler. Single-cell RNA-sequencing of Herpes simplex virus 1-infected cells identifies NRF2 activation as an antiviral program. *bioRxiv*, page 566992, 2019.
47. Caleb McKinney, Jiri Zavadil, Christopher Bianco, Lora Shiflett, Stuart Brown, and Ian Mohr. Global reprogramming of the cellular translational landscape facilitates cytomegalovirus replication. *Cell Rep.*, 6(6):1175, March 2014.
48. Jesper B Andersen, Krystyna Mazan-Mamczarz, Ming Zhan, Myriam Gorospe, and Bret A Hassel. Ribosomal protein mRNAs are primary targets of regulation in RNase-L-induced senescence. *RNA Biol.*, 6(3):305–315, July 2009.
49. Emma Abernathy and Britt Glaunsinger. Emerging roles for RNA degradation in viral replication and antiviral defense. *Virology*, 479-480:600–608, May 2015.
50. G T Spear, N S Lurain, C J Parker, M Ghassemi, G H Payne, and M Saifuddin. Host cell-derived complement control proteins CD55 and CD59 are incorporated into the virions of two unrelated enveloped viruses. human T cell leukemia/lymphoma virus type I (HTLV-I) and human cytomegalovirus (HCMV). *J. Immunol.*, 155(9):4376–4381, November 1995.
51. Boris Bogdanow, Henry Weisbach, Jens von Einem, Sarah Straschewski, Sebastian Voigt, Michael Winkler, Christian Hagemeier, and Lüder Wiebusch. Human cytomegalovirus tegument protein pp150 acts as a cyclin A2-CDK-dependent sensor of the host cell cycle and differentiation state. *Proc. Natl. Acad. Sci. U. S. A.*, 110(43):17510–17515, October 2013.
52. Laura Hertel and Edward S Mocarski. Global analysis of host cell gene expression late during cytomegalovirus infection reveals extensive dysregulation of cell cycle gene expression and induction of pseudomitosis independent of us28 function. *Journal of virology*, 78(21):

11988–12011, 2004.
53. Edward S Mocarski, Jr, Thomas Schenk, Paul D Griffiths, and Robert F Pass. Cytomegaloviruses. In Peter M Howley David M. Knipe, editor, *Fields Virology*, pages 1960–2014. Lippincott Williams & Wilkins, June 2013.
54. Uta Müller-Kuller, Mania Ackermann, Stephan Kolodziej, Christian Brendel, Jessica Fritsch, Nico Lachmann, Hana Kunkel, Jörn Lausen, Axel Schambach, Thomas Moritz, and Manuel Grez. A minimal ubiquitous chromatin opening element (UCOE) effectively prevents silencing of juxtaposed heterologous promoters by epigenetic remodeling in multipotent and pluripotent stem cells. *Nucleic Acids Res.*, 43(3):1577–1592, February 2015.
55. John G Doench, Nicolo Fusi, Meagan Sullender, Mudra Hegde, Emma W Vaimberg, Katherine F Donovan, Ian Smith, Zuzana Tothova, Craig Wilen, Robert Orchard, Herbert W Virgin, Jennifer Listgarten, and David E Root. Optimized sgRNA design to maximize activity and minimize off-target effects of CRISPR-Cas9. *Nat. Biotechnol.*, 34(2):184–191, February 2016.
56. Eva Maria Borst, Gabriele Hahn, Ulrich H Koszinowski, and Martin Messerle. Cloning of the human cytomegalovirus (HCMV) genome as an infectious bacterial artificial chromosome in Escherichia coli: a new approach for construction of HCMV mutants. *J. Virol.*, 73(10): 8320–8329, October 1999.
57. Joshua G Dunn and Jonathan S Weissman. Plastid: nucleotide-resolution analysis of next-generation sequencing and genomics data. *BMC Genomics*, 17(1):958, November 2016.
58. L Van Der Maaten and G Hinton. Visualizing high-dimensional data using t-sne. journal of machine learning research. *J. Mach. Learn. Res.*, 9:26, 2008.
59. Raul Garreta and Guillermo Moncecchi. *Learning scikit-learn: Machine Learning in Python*. Packt Publishing Ltd, November 2013.
60. Etienne Becht, Leland McInnes, John Healy, Charles-Antoine Dutertre, Immanuel W H Kwok, Lai Guan Ng, Florent Ginhoux, and Evan W Newell. Dimensionality reduction for visualizing single-cell data using UMAP. *Nat. Biotechnol.*, December 2018.
61. Xiaojie Qiu, Qi Mao, Ying Tang, Li Wang, Raghav Chawla, Hannah A Pliner, and Cole Trapnell. Reversed graph embedding resolves complex single-cell trajectories. *Nature methods*, 14(10):979, 2017.
62. Jeffrey Heer, Nicholas Kong, and Maneesh Agrawala. Sizing the horizon: the effects of chart size and layering on the graphical perception of time series visualizations. In *Proceedings of the 27th international conference on Human factors in computing systems - CHI 09*, page 1303, New York, New York, USA, 2009. ACM Press.
63. Eain Murphy, Isidore Rigoutsos, Tetsuo Shibuya, and Thomas E Shenk. Reevaluation of human cytomegalovirus coding potential. *Proc. Natl. Acad. Sci. U. S. A.*, 100(23):13585–13590, November 2003.

Materials and Methods

Cell and virus culture

Human foreskin fibroblasts (HFFs; CRL-1634) and HCMV (strain Merlin; VR-1590) were purchased from the American Tissue Culture Collection. HFFs were cultured in DMEM, supplemented with 10 % FBS and penicillin-streptomycin. HCMV stocks were expanded by two rounds of propagation on HFFs and titered by serial dilution. For stable expression of the CRISPRi/n machineries in HFFs, we modified established lentiviral (d)Cas9 expression vectors (13) by inserting a minimal ubiquitous chromatin opening element (UCOE) (54) upstream of the SFFV promoter, resulting in pMH0001 (UCOE-SFFV-dCas9-BFP-KRAB) and pMH0004 (UCOE-SFFV-Cas9-BFP). The UCOE prevented epigenetic silencing that affected the original constructs.

Pooled CRISPR screening

The HCMV tiling library was designed to contain sgRNAs targeting every single of the 33,465 PAMs in the HCMV Merlin genome (NCBI NC_006273.2), as well as 533 non-targeting controls (Table S1). It was synthesized and cloned into a lentiviral vector (Addgene #84832) as previously described (13, 14). For targeting host genes, we used the human CRISPRi v2 library (Addgene #83969) (14), and the K. Yusa *et al.* human knockout CRISPR v1 library (Addgene #67989) (31), respectively. Libraries were packaged into lentiviruses and delivered into (d)Cas9-expressing HFFs at an MOI of 0.3–0.5, followed by puromycin selection. Pooled screens were carried out at 500–1,000 × coverage, i.e. ∼500–1,000 cells per library element per sample taken. A t_0 sample was harvested and the remaining cells either passaged normally, or infected with HCMV at an MOI of 0.5–1.0 (for the HCMV tiling screens) or 0.1 (for the host-directed screens). Infected flasks were washed with PBS and given fresh media at days 3, 5, 7 post infection to remove dead cells, and harvested at day 9–10. Genomic DNA was extracted and digested with MfeI (pCRISPRia v2-based libraries) or HindIII (Yusa *et al.* library) to release a fragment containing the sgRNA cassette, followed by gel-based extraction, PCR amplification and deep sequencing as described (14). Raw count data were normalized for read depth and a small constant added to account for missing values. Phenotypes of individual sgRNAs were expressed as $\log_2$-transformed ratios of adjusted read counts between samples (Table S2). We calculated the mean of all sgRNAs specific to each host gene. For the HCMV tiling screen, we calculated a rolling average in a 200 bp window, with the average of all non-targeting sgRNAs defining the baseline.

Single-cell RNA-seq

For the single-cell infection time course, WT HFFs were lentivirally transduced with barcoded Perturb-seq vectors to encode the experimental condition (pBA571, Addgene #85968; Table S3, sheet 2), followed by puromycin selection. Cells were seeded at a density of 250,000 per well of a 12-well plate and infected with an MOI of 0.5 (low) or 5.0 (high). Infection times were staggered so that all time points for a given MOI were harvested in parallel, pooled, prepared for single-cell transcriptomics using one lane each of the Chromium Single Cell 3′ Gene Expression Solution v2 according to manufacturer's instructions (10x Genomics), and sequenced on a NovaSeq platform (Illumina) at ∼100,000 reads/cell. Barcodes encoding the experimental condition were PCR-amplified from the final library and sequenced separately as described (29).

Perturb-seq

For the host-directed CRISPRi Perturb-seq experiment, we initially selected 53 candidate genes by their strong protective or sensitizing phenotypes in the pooled screen (one gene was later removed during analysis, see below). We manually picked the two best performing sgRNAs for each candidate. Additionally, we added six non-targeting control constructs (targeting GFP, which is not present in our HFFs). For the host- and virus-directed CRISPRn Perturb-seq experiment, we selected a set of 21 host factors, of which 19 were already among the targets CRISPRi Perturb-seq experiment, had no strong essentiality knockout phenotypes and comparable protective or sensitizing phenotypes in both the pooled host-directed CRISPRi and CRISPRn screens (see Fig. S3). We further added PDGFRA and FLCN, both of which were strong hits in the pooled CRISPRn screen. For each host target, we manually picked the two best performing sgRNAs. In addition, we selected 31 viral targets with strong protective or sensitizing phenotypes, corresponding to the three strongest modules identified in the HCMV tiling screen (see Fig. S2). From the tiling screen, we selected the two highest-ranking sgRNAs for each target gene based on the following scoring system: From the pool of unique sgRNAs falling within the gene boundaries and having a Doench score (55) of >0.5, we calculated the absolute average phenotype across replicates and subtracted a penalty defined as the difference between replicates plus the average absolute essentiality phenotypes (on a $\log_2$ scale). We designed a number of safe-targeting control sgRNAs targeting intergenic DNA in the US2–US12 region. This region was selected based on its near-neutral phenotypes in the tiling screen (Fig. S2), a lack of essential genes (9, 10), and its comparatively large spaces between consensus genes. Further, in some bacterial artificial chromosome (BAC) constructs harboring HCMV genomes, this region has been replaced by the BAC backbone, underlining its non-essential nature during infection in tissue culture (56). We picked five sgRNAs based on their Doench scores from a pool of unique sgRNAs targeting the intergenic regions and having survival and essentiality phenotypes of <0.5 ($\log_2$ scale) in all replicates. In addition, we included four control sgRNAs directed against safe-harbor loci in the host genome that we repurposed from gene knock-in applications.

All sgRNAs were synthesized as individual oligo pairs (IDT) and cloned into a barcode library containing plasmid pool (pBA571, Addgene #85968), thereby linking each sgRNA to a unique guide barcode contained within the 3′-UTR of the puromycin resistance gene (29). Barcodes were validated to not contain homo-oligomers or sequences resembling transcription termination signals. All sgRNA and barcode sequences are listed in Table S3.
sgRNAs vectors were packaged into lentiviruses individually, titered separately and pooled to ensure equal representation. We delivered the library into (d)Cas9-expressing HFFs at an MOI of 0.3 followed by puromycin selection. Cells were seeded at 250,000 per well of a 12-well plate and infected with HCMV at an MOI of 0.5 (for the CRISPRi host-directed experiment) or 5.0 (for the CRISPRn host and virus-directed experiment). Cells were harvested in the uninfected state (0 h) and at 24, 48 and 72 h.p.i. We aimed at a representation of each sgRNA by ∼100 cells per time point. Cells were collected and prepared for sgRNA-seq using the 10x Chromium platform as described above for the single-cell infection time course. Libraries were sequenced on a HiSeq4000 or NovaSeq platform (Illumina) at ∼40,000 reads/cell.

Single-cell data analysis

Raw sequencing data were submitted to 'cellranger' (10x Genomics) according to the manufacturers instructions. We compiled a reference transcriptome from the hg19 human genome and a custom assembly of HCMV coding transcripts based on our previous ribosome profiling dataset (3) as distributed as part of the 'Plastid' python library demo dataset (57). We manually added four well-established lncRNA transcripts (RNA1.2, 2.7, 4.9, 5.0). Internal ORFs were removed as they would create ambiguous mappings, as were ORFs overlapping with the aforementioned lncRNAs. Cells retained in the final dataset had to cross the default cellranger quality thresholds, as well as have one unique lentiviral barcode assigned with high confidence (29). During data analysis of the perturb-seq experiments, three CRISPRn sgRNAs targeting host genes were removed computationally because they were found to be inactive, as seen by lack of transcriptional responses and viral load patterns similar to control sgRNAs. One host gene, RBBP5, was similarly excluded from both the CRISPRi and CRISPRn datasets as it became apparent that its knockdown/knockout causes differentiation of cells and a strong transcriptional response, rather than true protection against infection.
Viral loads were calculated as the fraction of total UMIs per cell mapping to viral genes.
Gene expression was normalized first in each cell by the total unique molecular identifiers (UMIs) per cell and then z-scored on a per-gene basis across all cells. Human genes represented by <10,000 UMIs across all cells, as well as viral genes represented by <5,000 UMIs were removed before hierarchical clustering. For heatmap representations of gene expression as a function of viral load, cells were binned by viral load and gene-level expression values averaged in each bin. Bin widths of 2 % or 10 % were selected depending on the available number of cells, with the lower bound indicated in the respective figures.
Cell cycle phases were scored based on marker genes as described (29). Using a similar approach we calculated an IFN score by summing and subsequently z-scoring the relative expression values of the following set of robustly quantified ISGs (PSMB8, PSMB9, PSME1, PSME2, ISG15, ISG20, IRF7, MX1, MX2, GBP1, GBP2, GBP3, IFI6, IFI44, IFI35, IFI16, IFI27, IFIH1, IFI44L, IFIT1, IFIT2, IFIT3, IFIT5, IFITM1, IFITM2, IFITM3, EIF2AK2, OAS1, OAS2, OAS3, CNP, PLSCR1, BST2, BTN3A2, XAF1, CASP1, CASP4, CASP7, GSDMD).
Dimensionality reduction was performed by t-SNE (58) implemented in scikit-learn (59) or UMAP (60) implemented in Monocle (61). Trajectories were based on UMAP projections. To determine trajectories, selected cells were ranked by viral load and the geometric position of cells averaged in a sliding window that was shifted in increments of 0.2 window sizes. Window sizes were selected based on the total number of available cells: Perturb-seq experiments: 100 cells; unperturbed cells, dominant trajectory: 500 cells, alternate trajectory: 50 cells.

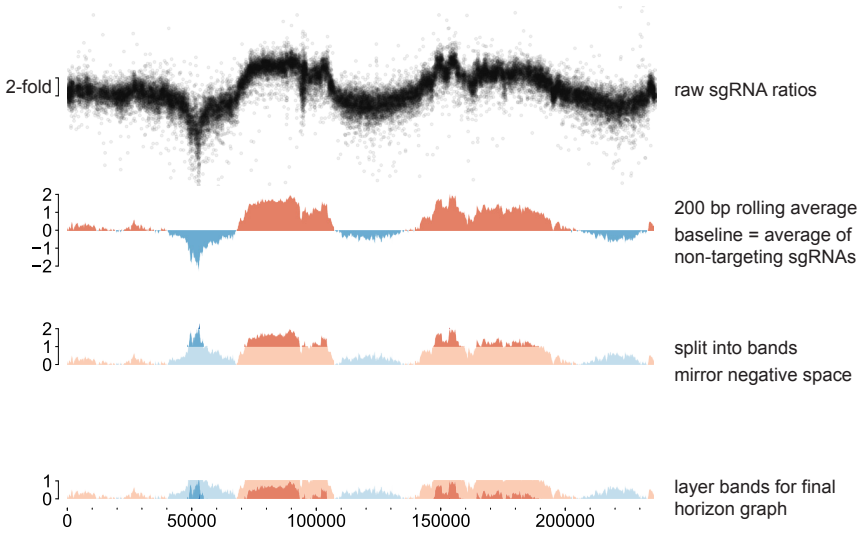

Fig. S1. Data processing for the HCMV tiling screen.
We calculated $\log_2$ ratios of each individual sgRNA in the surviving over the t_0 populations. Ratios were averaged in a sliding 200 bp window. The average of the ratios of the non-targeting sgRNA population was set as the baseline. The plot was then colored based on the sign of the average phenotype (reds: positive sign, protective phenotype; blues: negative sign, sensitizing phenotype) and layered in bands of decreasing lightness, one $\log_2$ unit wide. The negative space was mirrored on the baseline, and bands were stacked for the final horizon plot representation (62). For high resolution see Fig. S2.

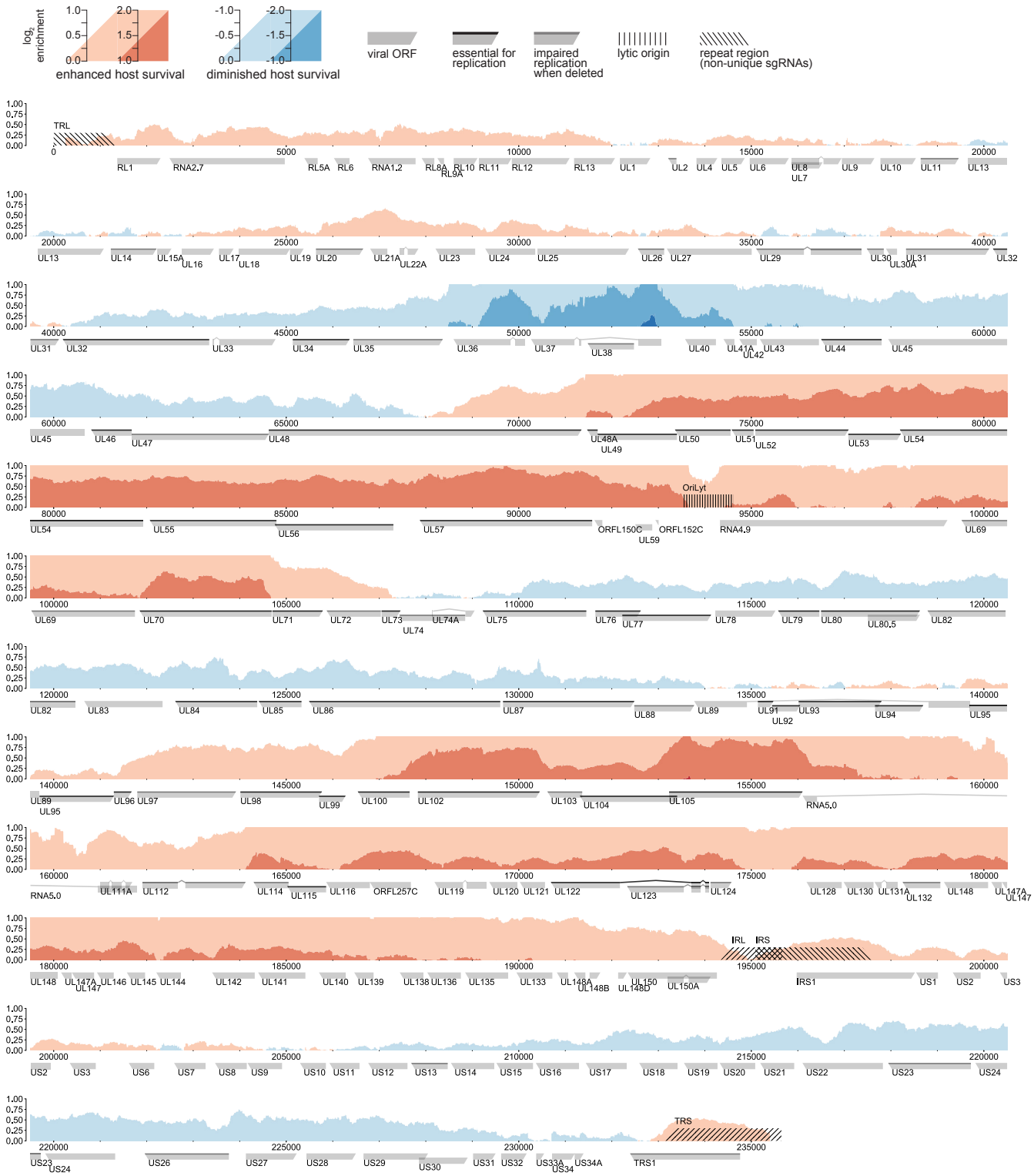

Fig. S2. High-resolution phenotypic landscape of the HCMV genome.

Horizon graph representation (62) of the phenotypic landscape with mirrored and stacked bands. Shades of blue denote sensitization to host cell death, shades of red denote protection from cell death upon HCMV genome cleavage. Major features of the HCMV genome are annotated. sgRNAs targeting internal and terminal repeat regions (hashed) typically have multiple target sites and likely result in higher-order fragmentation of the HCMV genome, exacerbating their respective phenotypes. Viral ORFs are classified by their essentiality for viral replication based on Dunn *et al.* (9) ORFL150C, ORFL151C (originally named UL59, but thought to not be expressed as a protein (63), causing it to be dropped from the consensus annotation), and ORFL152C were the only short ORFs with strong phenotypes in areas of the genome devoid of consensus genes. UL48 was the only gene that showed a substantial phenotype gradient within its gene body: Cutting the N-terminal region caused mild sensitization to death upon infection, whereas cutting the C-terminus had the opposite effect.

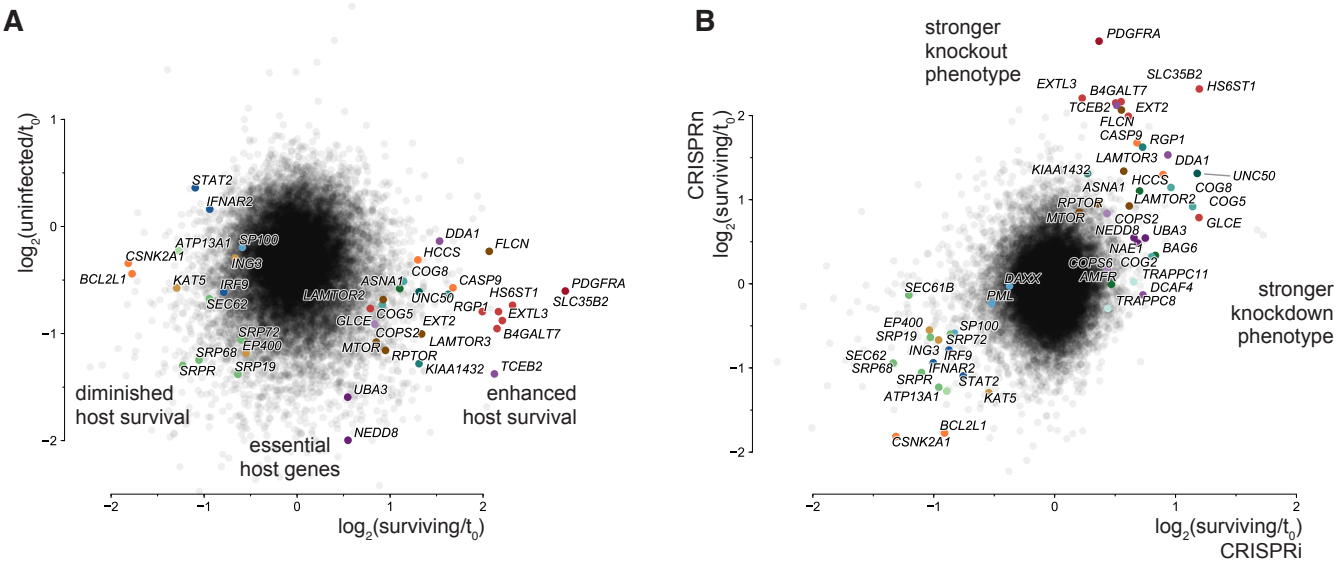

Fig. S3. Host-directed CRISPRn screen results and CRISPRi/n comparison.
(**A**) Results of host-directed CRISPRn screen displayed as a scatter plot of average gene essentiality (i.e. infection-independent phenotype; y-axis) vs. protection/sensitization to death upon HCMV infection (i.e. infection-dependent phenotypes; x-axis). Note that due to the experimental design of the screen, the apparent gene essentiality phenotypes are underestimating the real essentiality because t_0 refers to the beginning of HCMV infection, not lentiviral delivery of the sgRNA library. (**B**) Direct comparison of CRISPRi and CRISPRn phenotypes for host targets represented in both libraries. Hits involved in viral adhesion and entry, as well as host cell survival or apoptosis are more pronounced in the CRISPRn screen. Cullin/RING pathway members and some vesicle trafficking factors were only resolved in the CRISPRi screen.

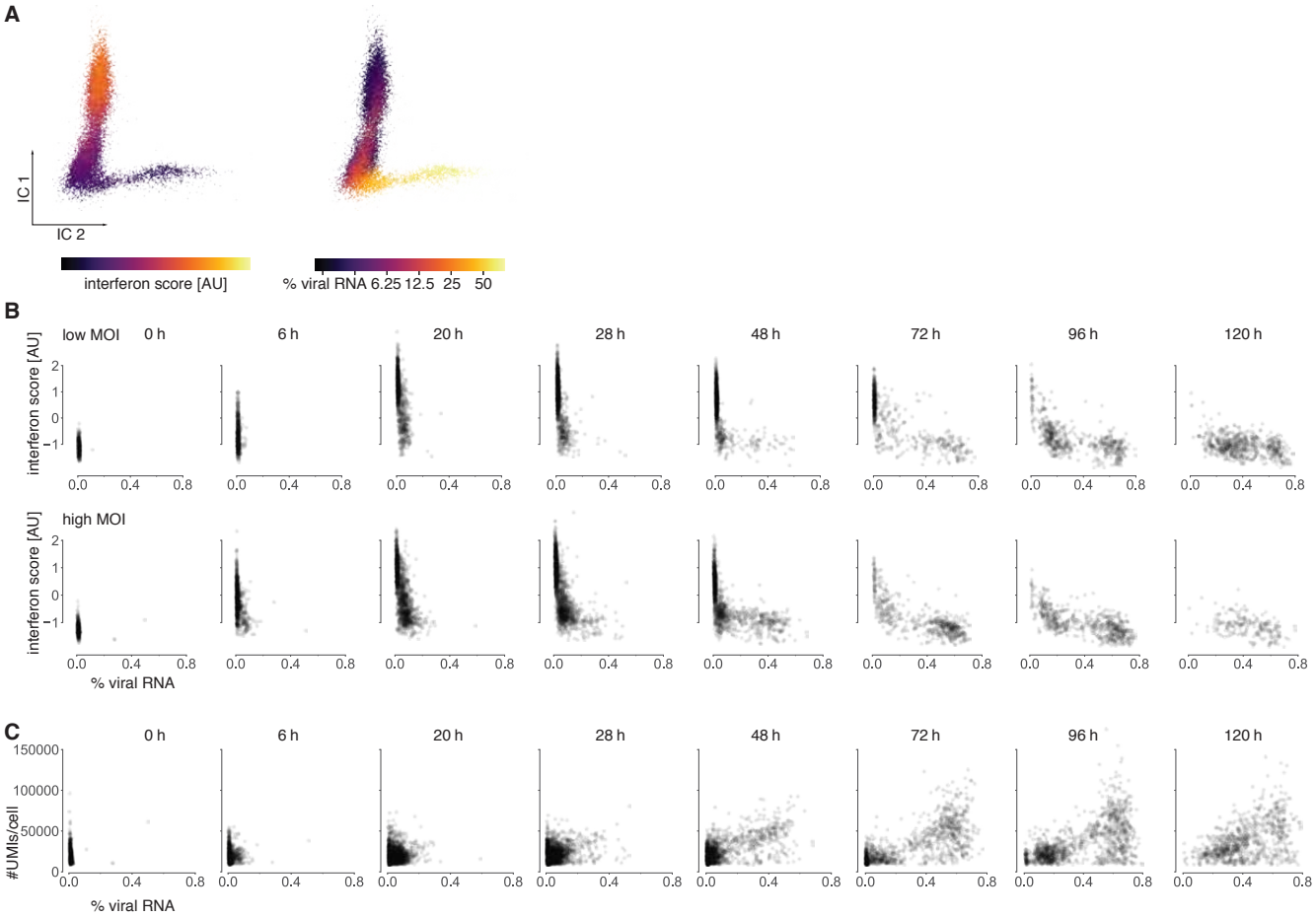

Fig. S4. Interferon activation and viral load are the main sources of variability between cells.
(**A**) Independent component (IC) analysis shows that the largest sources of variability, i.e. components 1 and 2, can be explained by the extent of expression of interferon-stimulated genes (represented by the interferon score; see Materials and methods) and the viral load (i.e. the fraction of viral RNA), respectively. (**B**) Interferon scores of individual cells plotted against their viral loads, broken down by experimental time point and multiplicity of infection (MOI). The majority of cells mount an interferon response as soon as a minority of cells become infected (at 6 h.p.i.), likely through paracrine signaling. In early infected cells, interferon activation is then rapidly suppressed (compare 20 and 28 h.p.i) and returns almost to baseline in later stage infected cells. Differences between low and high MOI are most apparent at 72 h.p.i, where almost all cells challenged with a high MOI are infected whereas an uninfected subpopulation remains after low MOI infection. (**C**) Number of unique molecular identifiers (UMIs) per cell as a function of viral load, broken down by experimental time point. UMI counts can serve as a proxy for total RNA content per cell, and are positively correlated with viral load, indicating a higher cellular RNA content of infected cells.

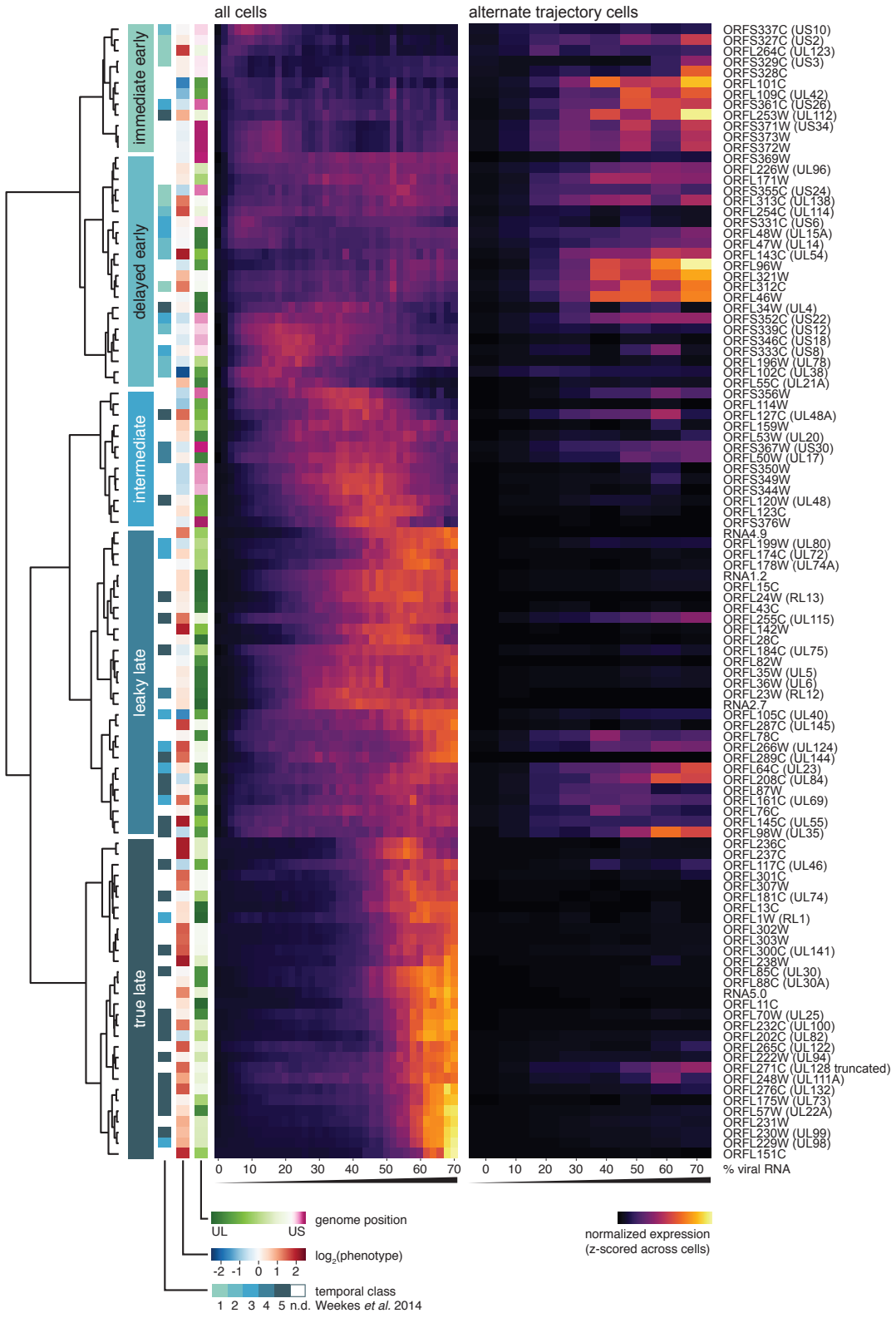

Fig. S5. Expression pattern of viral genes as a function of viral load.
Cells were binned and averaged in viral load increments of 2 % (all cells, left) and 10 % (alternate trajectory cells, right) and viral transcripts clustered based on the pattern observed with all cells. This is a high-resolution version of Fig. 2D, E. Viral transcripts are annotated by their temporal class as described by Weekes *et al.* (4), by their phenotype in the HCMV tiling screen (see Fig. 1B and Fig. S2), and by their position in the viral genome (green, unique long (UL) branch; purple, unique short (US) branch; increasing saturation towards the terminal regions). Note the relationship between a gene's temporal class and its phenotype in the pooled screen: True-late and leaky-late genes predominantly showed protective phenotypes, whereas earlier classes also contained sensitizing genes.

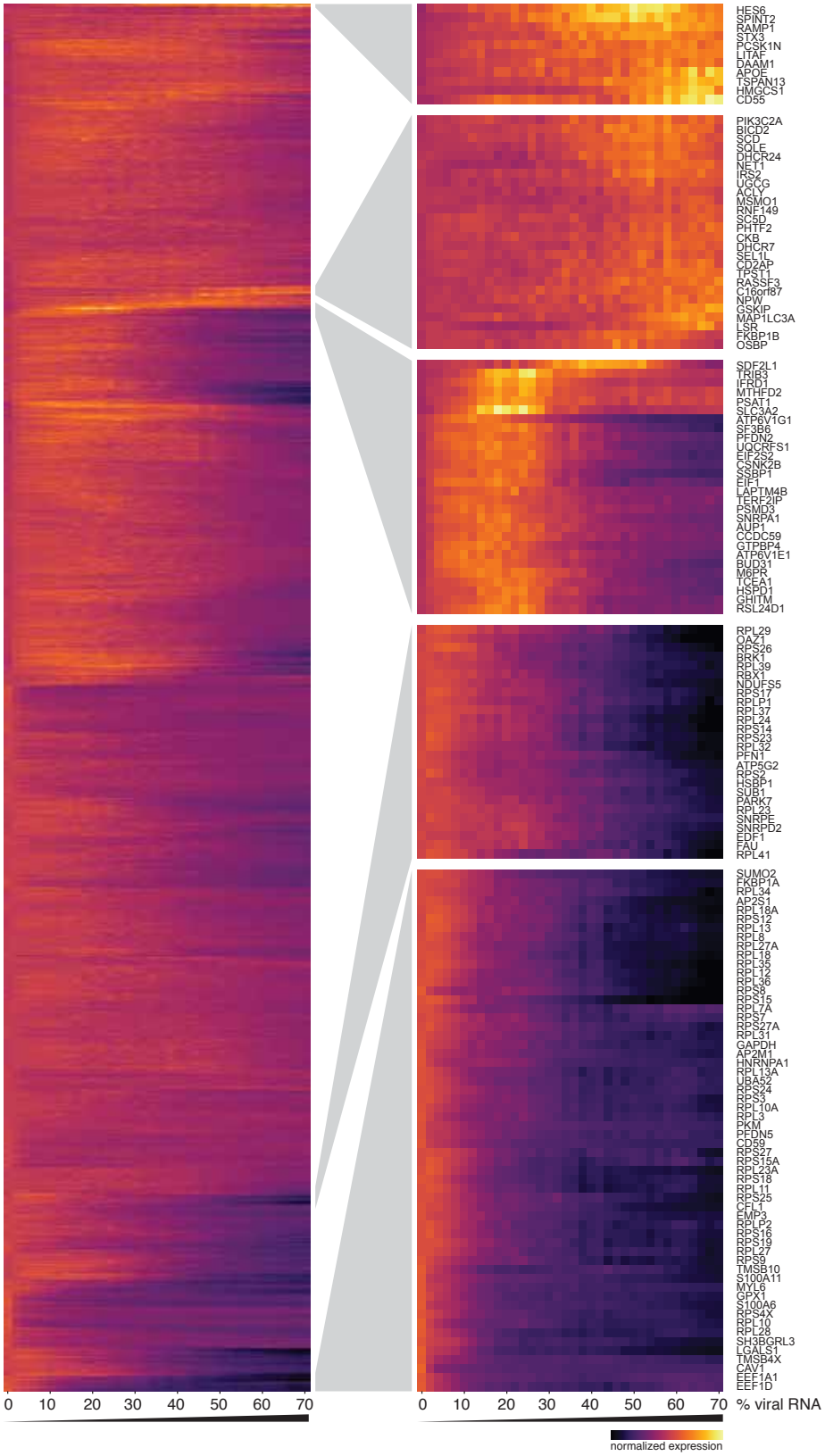

Fig. S6. Expression pattern of host genes as a function of viral load.
Cells were binned and averaged in viral load increments of 2 % and host transcripts clustered hierarchically. The dominant pattern is, as expected, for host transcripts to decrease in abundance according to the increase in viral load. A minority of transcripts stand out by either increasing with viral load (upper two blown-up clusters), peaking at medium viral load (middle cluster), or decreasing over-proportionally (bottom two clusters). Upregulated transcripts encode membrane proteins, trafficking factors and enzymes involved in lipid synthesis. Downregulated transcripts include highly abundant housekeeping transcripts such as those of ribosomal proteins, elongation factors, or GAPDH.

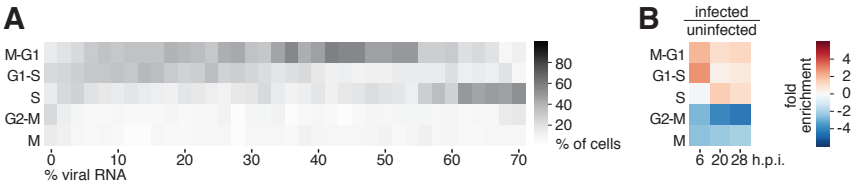

Fig. S7. Shifts in the cell cycle distribution of infected cells.
(**A**) Distribution of cells across cell cycle phases as a function of viral load. Infected cells assume a G1-like state and switch to an S-like state at ∼55 % of viral load, which also marks the onset of late-gene expression and viral genome replication (compare Figs. 2D, S5). (**B**) Ratio of cell cycle distributions of early infected cells (defined here as 2–10 % viral load) over uninfected cells (<1 % viral load) as a function of experimental time. Cells in M-G1 and G1-S are the ones permissive towards initial progression of infection (at 6 h.p.i.), and their progression towards G2/M phase is then suppressed (at 20–28 h.p.i.).

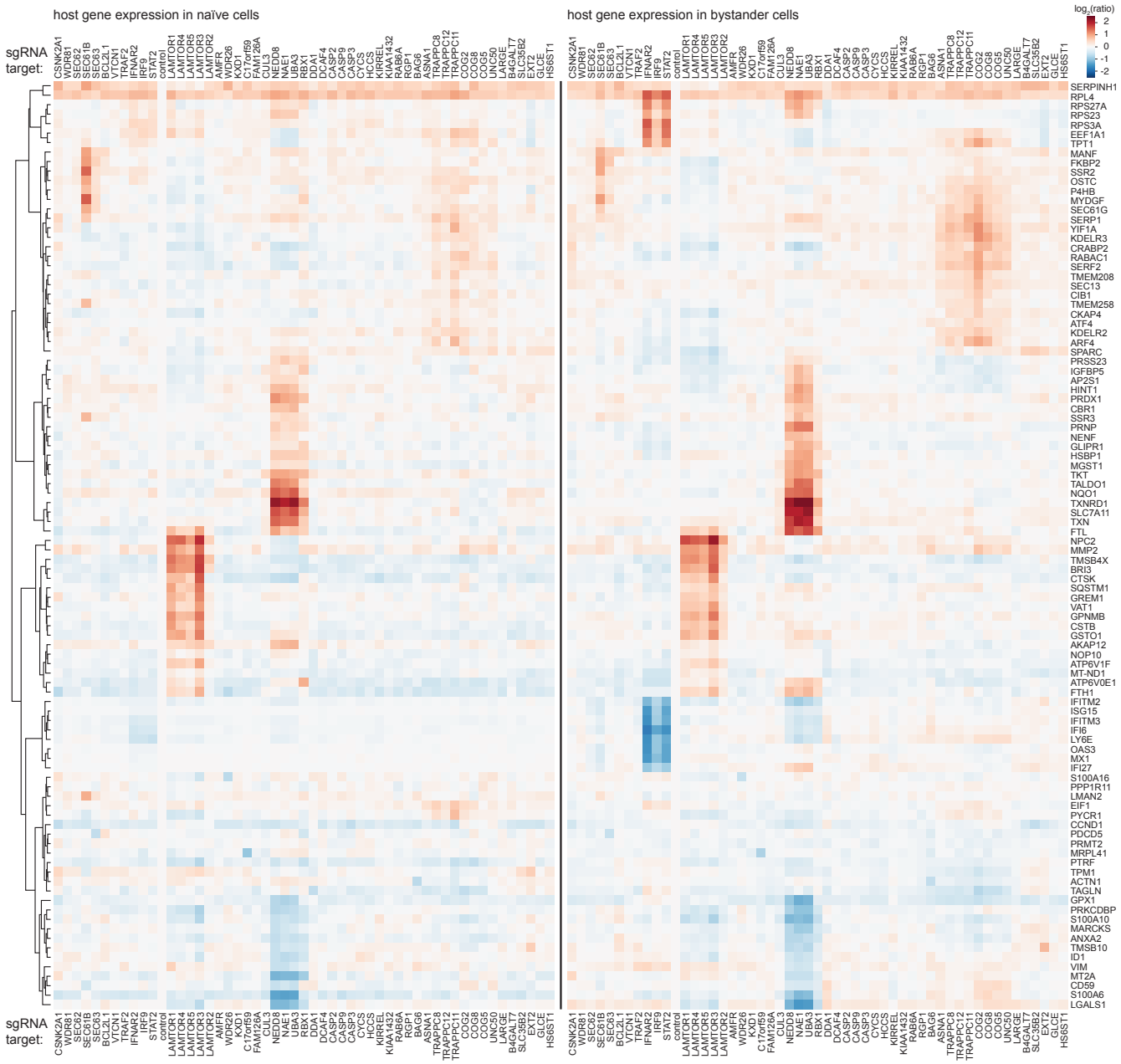

Fig. S8. Transcriptional response to host factor knockdown in naïve and bystander cells.
Hierarchical clustering of the expression a representative set of 98 host genes that show the strongest responses to either of the genetic perturbations in the CRISPRi perturb-seq experiment, normalized by control cells. The left panel shows data from naïve cells (defined here as cells from the 0 h time point). The right panel shows data from bystander cells (defined here as cells with <1 % viral load from the 24–72 h.p.i. time points) and is a higher resolution version of Fig. 3C. The interferon response characteristic of bystander cells is suppressed by knockdown of IFN pathway members IFNAR2, IRF9 and STAT2. Knockdown of the susceptibility factors SEC61B and SEC62 show mild suppression of ISGs as well. Knockdown of NEDD8, NAE1, UBA3 and RBX1 cause a transcriptional response that overlaps in part with the IFN-responsive genes, but with varying directionality.

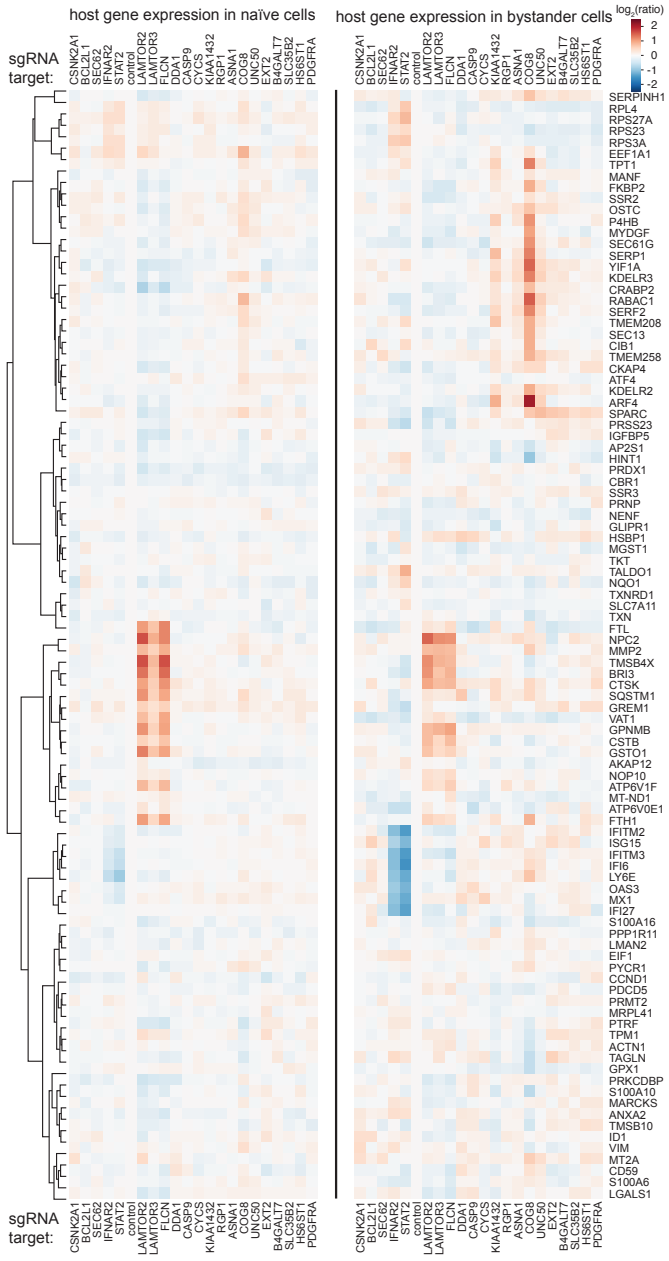

Fig. S9. Transcriptome response to host factor knockout in naïve and bystander cells.
Conceptually related to Fig. S8, showing the same clustering of 98 representative host genes in response to knockout of host factors in the CRISPRn Perturb-seq experiment. The left panel shows data from naïve cells; the right panel shows data from bystander cells, both defined as in Fig. S8. Patterns and directionality of the transcriptional responses are in agreement between host factor knockdown and knockout.

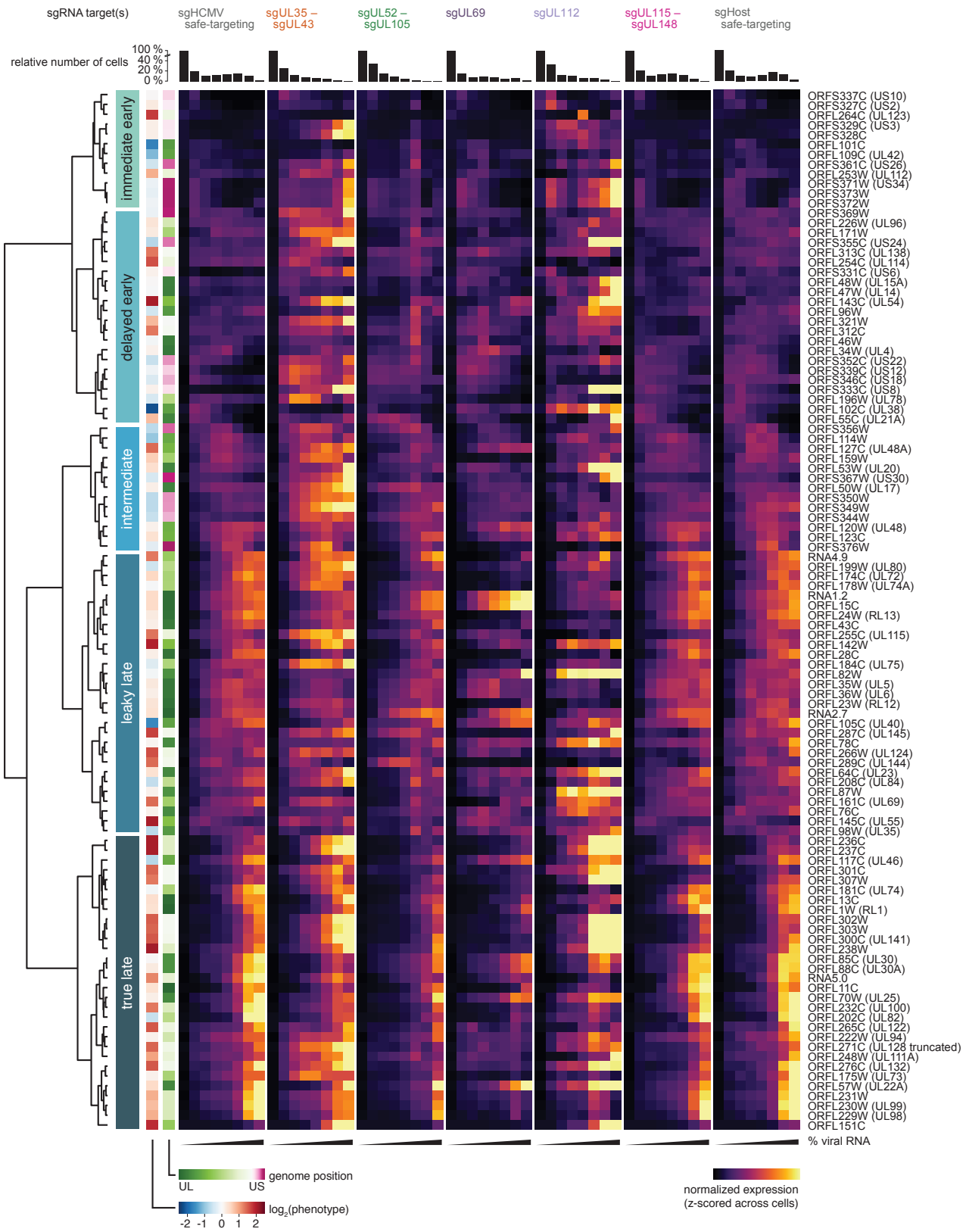

Fig. S10. Patterns of viral gene expression along the different groups of trajectories.
Cells were binned and averaged in viral load increments of 10 % for all cells belonging to a given group of trajectories, and clustered based on the pattern observed in unperturbed cells to reflect their membership in the default temporal classes. This is a high-resolution version of Fig. 4E. Viral transcripts are annotated by their phenotype in the HCMV tiling screen (see Fig. 1B and Fig. S2), and by their position in the viral genome (green, unique long (UL) branch; purple, unique short (US) branch; increasing saturation towards the terminal regions).

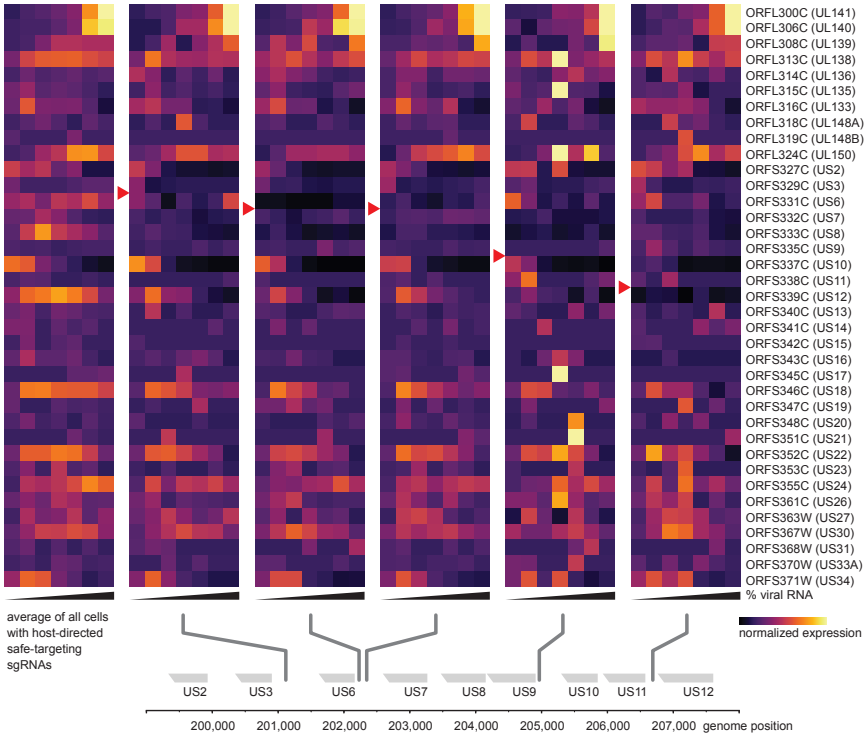

Fig. S11. Effect of safe-targeting sgRNAs on expression of genes adjacent to the cut sites.
The clustering shows the viral gene expression patterns as a function of viral load, broken down by individual safe-targeting sgRNA. The sgRNAs were designed to target the comparatively large intergenic sequences in the non-essential US2–US12 region of the HCMV genome, and do not change the overall expression trajectories of infected cells. Viral genes are arranged in the order they are encoded in the genome. Red arrows denote which genes are adjacent to the cut sites in the expression heatmaps. Two of the five safe-targeting sgRNAs, one targeting a site immediately upstream of US6, and one between US11 and US12, show markedly reduced expression of an adjacent gene (US6 and US12, respectively). Note that another sgRNA targeting the US6–US7 intergenic space further away from the US6 N-terminus shows a much weaker effect on US6. All safe-targeting sgRNAs caused reduced expression of US6, US8 and US12, the most strongly expressed genes in a $\sim$5 kb window around the cut sites.